AN INDUCED TORQUE STUDY OF $Hg_{3-\delta}AsF_6$

AN INDUCED TORQUE STUDY OF $Hg_{3-\delta}AsF_6$

by

RAYMOND J. DINSER, B.Sc.

A Thesis

Submitted to the School of Graduate Studies

in Partial Fulfilment of the Requirements

for the Degree

Master of Science

McMaster University

July 1982

MASTER OF SCIENCE (1982)
(Physics)

McMASTER UNIVERSITY
Hamilton, Ontario

TITLE: An Induced Torque Study of $Hg_{3-\delta}AsF_6$

AUTHOR: Raymond J. Dinser, B.Sc. (University of Windsor, Canada)

SUPERVISOR: Professor W.R. Datars

NUMBER OF PAGES: vii, 55

ABSTRACT

Under certain conditions, an induced torque measurement is a measure of the ratio of the resistivity to the square of the Hall constant. Induced torque measurements can be directly related to the connectivity of the Fermi surface.

A modulation technique for measuring induced torque is justified theoretically, and an instrument employing this technique is characterized. Operational limitations on parameters such as sample resistivity and modulation rate are specified. A new procedure is proposed to extract more information from induced torque measurements. This procedure would allow the measurement of resistivity and Hall constant of ellipsoidal samples. The procedure is untested but appears to be feasible.

Observations of the induced torque of $Hg_{3-\delta}AsF_6$ show that the Fermi surface supports an open orbit in one direction. This is discussed in the context of a model (Razavi et al., 1979), which has Fermi surface cylinders of common direction. This is based on conduction in Hg chain directions, which lie in only two directions. At magnetic fields greater than 3.0 Tesla, magnetic breakdown is observed. A Brillouin zone constructed using Hg chain symmetry and crystal parameters yields reciprocal lattice vectors compatible with the observed magnetic breakdown, The model is confirmed but a refinement is needed to allow an undulation of the Fermi surface cylinders.

ACKNOWLEDGEMENT

I would like to thank my supervisor, Dr. W.R. Datars for his suggestions and encouragement through the course of this work. Dr. Zaven Altounian assumed much the same task; their concern and help is much appreciated.

Erwin Batalla, Feriedoon Razavi, Gunter Scholz and Duane Chartier have all contributed to my understanding of the material. Mr. Chartier also synthesized and mounted the crystals.

Clarence Verge built and maintained the magnetometer. He also provided invaluable technical assistance and advice.

My own family, the Clifford McMahon family, Tom Znotins, Lynne Soderholm, Phil Coulter, and too many friends to mention provided vital moral support. My parents deserve a special note of thanks.

Mrs. Kathy Noon typed the manuscript very quickly and accurately.

Personal financial support from McMaster University is gratefully acknowledged. This research was supported by the National Sciences and Engineering Research Council.

TABLE OF CONTENTS

LIST OF FIGURES

LIST OF TABLES

CHAPTER 1

INTRODUCTION

$Hg_{3-\delta}AsF_6$ is a metallic compound first discovered by R.J. Gillespie and P.K. Ummat (1971), and grown as a single crystal by Cutforth and coworkers (1975). The structure was determined by x-ray diffraction (Brown et al., 1974) to consist of a tetragonal lattice of octahedral AsF_6^- anions with mercury atoms arranged in linear chains which lie in only two directions.

Resistivity measurements (Cutforth et al, 1976) show a highly anisotropic conductivity of order 125 at room temperature. Further resistivity (Cutforth et al. 1975, Chaing et al. 1977), optical (Koteles et al. 1976, Peebles et al. 1977) and thermopower (Scholz et al., 1977) measurements confirmed that the conductivity is highly anisotropic.

An induced torque is that torque which opposes the rotation of a metallic sample in an applied magnetic field due to the interaction between the applied field and the moment due to induced eddy currents. The current density is a function of resistivity tensor elements (Visscher and Falicov, 1970): this function is derived in Chapter 2.

At low temperatures and high magnetic fields $\vec{B}_0$, induced torque measurements are very sensitive to the presence of open orbits in the Fermi surface perpendicular to the magnetic field $\vec{B}_0$.

The induced torque magnetometer employs a special modulation technique. The function and uses of the magnetometer are detailed in

Chapter 3: the use of modulation is justified in Chapter 4. Modifications to the magnetometer to simplify its use and to obtain more information about the sample are proposed in Chapter 3.

This method was used to study the open orbits of $Hg_{3-\delta}AsF_6$. The experimental results are presented in Chapter 6 and are interpreted in terms of the Fermi surface model developed by Razavi et al., (1979) in Chapter 7.

The purpose of this thesis is to study the induced torque method and to use this method to obtain more information about the Fermi surface of $Hg_{3-\delta}AsF_6$.

CHAPTER 2

THEORY OF INDUCED TORQUE

Induced torque measurements exploit the eddy currents induced in a metal when it is rotated in a magnetic field. Such eddy currents produce a magnetic field $\vec{M}$ which couples to the applied field $\vec{B}_o$, resulting in a torque $\vec{N}$. The component of $\vec{N}$ opposing the rotation of the sample is known as an induced torque.

The torque was calculated by Landau and Lifshitz (1960) for an isotropic metal with a magnetic-field-independent conductivity. This was extended to the more interesting case where conductivity is both field dependent and a tensor by Lass and Pippard (1970), and independently by Visscher and Falicov (1970). Both treatments assume uniform rotation of the sample. The treatment of Visscher and Falicov is presented in Section II.1.

II.1 The Torque Induced by Uniform Rotation

The torque $\vec{N}$ can be obtained by solving for eddy current density $\vec{J}$ using Maxwell's equations and boundary conditions.

Assuming a low rotation rate, Maxwell's equations reduce to the "quasistatic approximation"

$$\nabla \times \vec{E} = -\dot{\vec{B}} \tag{2.1}$$

$$\nabla \times \vec{H} = \varepsilon_o \vec{E} + \vec{J} \sim \vec{J} \tag{2.2}$$

This approximation is strictly true only in the static case, but is justified if $\dot{\vec{B}}$ is sufficiently slow. Defining $\lambda = cT$, where T is a characteristic time required for significant change in $\vec{B}$, and c is the speed of light in the material, we require that λ be much greater than the carrier mean free path or crystal dimensions (Hauser, 1971). In typical torque studies the time required for $\vec{B}$ to change direction by 0.02 radian ($\sim$ one degree) is on the order of one second. The condition on λ is easily fulfilled and (2.1) and (2.2) can be used.

The boundary condition on current $\vec{J}$ is that in the case of a spherical sample, at the surface,

$$\vec{J}.\vec{r} = 0 \tag{2.3}$$

The restriction to the case of spherical samples is not necessary. The problem has been solved by Lass (1976), for ellipsoidal samples, but this refinement is not discussed here.

With (2.3), the only restrictions necessary to assure uniqueness of the solution is

$$\nabla \cdot \vec{J} = \dot{\rho}_c = 0 \tag{2.4}$$

where $\dot{\rho}_c$ is the rate of change of electrical charge density. This is reasonable in the quasistatic regime: T is so much longer than typical carrier relaxation times that pockets of varying charge density cannot form. This does not exclude the possibility of helicon oscillations or other oscillations of the plasma.

The current density $\vec{J}$ is obtained by postulating

$$\vec{J} = \vec{t} \times \vec{r} \tag{2.5}$$

where $\vec{t}$ is unknown. Using the definition of the resistivity tensor

$$\vec{E} = \overleftrightarrow{\rho}\,\vec{J} \tag{2.6}$$

and Maxwell's equation (2.1)

$$\nabla \times \vec{E} = \nabla \times \overleftrightarrow{\rho}\,\vec{J} = \nabla \times \overleftrightarrow{\rho}\,(\vec{t}\times\vec{r}) = -\dot{\vec{B}} \tag{2.7a}$$

this can be solved algebraically

$$\vec{t} = [\mathrm{Tr}(\overleftrightarrow{\rho})\,\overleftrightarrow{I} - \overleftrightarrow{\rho}^{+}]^{-1} \cdot \dot{\vec{B}} \tag{2.7b}$$

where $\mathrm{Tr}(\overleftrightarrow{\rho})$ is the trace of $\overleftrightarrow{\rho}$, and $\overleftrightarrow{\rho}^{+}$ is the transpose.

$$[\mathrm{Tr}(\overleftrightarrow{\rho})\,\overleftrightarrow{I} - \overleftrightarrow{\rho}^{+}]^{-1} = \begin{pmatrix} (\rho_{yy} + \rho_{zz}) & -\rho_{yx} & -\rho_{zx} \\ -\rho_{xy} & (\rho_{xx} + \rho_{zz}) & -\rho_{zy} \\ -\rho_{xz} & -\rho_{yz} & (\rho_{xx} + \rho_{yy}) \end{pmatrix}^{-1}$$

Defining $\overleftrightarrow{\sigma}' \equiv [\mathrm{Tr}(\overleftrightarrow{\rho})\,\overleftrightarrow{I} - \overleftrightarrow{\rho}^{+}]^{-1}$, (2.9)

$$\vec{t} = \overleftrightarrow{\sigma}' \cdot \dot{\vec{B}}$$

The resultant torque can be found through the Lorentz force: for an element of volume $d^3\vec{r}$

$$d\vec{F} = (\vec{J} \times \vec{B})\, d^3\vec{r} \tag{2.10}$$

and $$d\vec{N} = \vec{r} \times d\vec{F} = \vec{r}\times(\vec{J} \times \vec{B})\, d^3\vec{r} \tag{2.11}$$

Substituting $\vec{J} = \vec{t} \times \vec{r}$ (2.5) and integrating over a sphere of radius R the torque is found to be

$$\vec{N} = \vec{t} \times \vec{B}\,\frac{4\pi R^5}{15} = \frac{-4\pi R^5}{15}\,\vec{B}_o \times \overleftrightarrow{\sigma}' \cdot \dot{\vec{B}} \tag{2.12}$$

Given $\vec{B}_o = B_o \hat{Z}$ (2.13a)

and $\vec{B} = B_o \Omega \hat{X}$ (2.13b)

where Ω is crystal rotation rate [see Figure (2.1)]

$$\vec{N} = \frac{-4\pi R^5}{15} B_o^2 \Omega \cdot \begin{pmatrix} \sigma_{yx}' \\ \sigma_{xx}' \\ o \end{pmatrix} \tag{2.14}$$

The torque is measured about the rotation axis, $\hat{Y}$. The induced torque is N_y,

$$N_y = \frac{-4\pi R^5}{15} B_o^2 \Omega \sigma_{xx}' \tag{2.15}$$

where $\sigma_{xx}' = ([Tr(\rho)\overleftrightarrow{I} - \overleftrightarrow{\rho}^+]^{-1})_{xx}$ (2.7b)

Induced torque measurements are useful in Fermi surface studies of single crystals at low temperatures if the high field limit $\omega_c\tau >> 1$ holds, where $\omega_c = \frac{eB_o}{m}$, the cyclotron frequency, and τ is the mean time between scattering events. If these criteria are met, electron dynamics is dominated by Fermi surface parameters and the applied field.

In the high field limit, assuming no longitudinal-transverse mixing ($\rho_{iz} = \rho_{zi} = 0$),

$$\sigma_{xx}' = \frac{\rho_{xx} + \rho_{zz}}{(\rho_{xx}+\rho_{yy})(\rho_{xx}+\rho_{zz}) + \rho_{yx}\rho_{xy}} \tag{2.16a}$$

This can often be approximated

$$\sigma_{xx}' \sim \frac{\rho_{xx}}{\rho_{xy}^2}$$

FIGURE 2.1: The geometry of rotation. The applied field $\vec{B}_o$ is taken to be in the $\vec{Z}$ direction. Rotation about the $\vec{Y}$ axis produces a change in the field in the $\vec{X}$ direction. $\dot{\vec{B}} = B_o \Omega \vec{X}$, where Ω is the rotation rate. The directions of the applied field and the rotation axis are unchanged throughout this work.

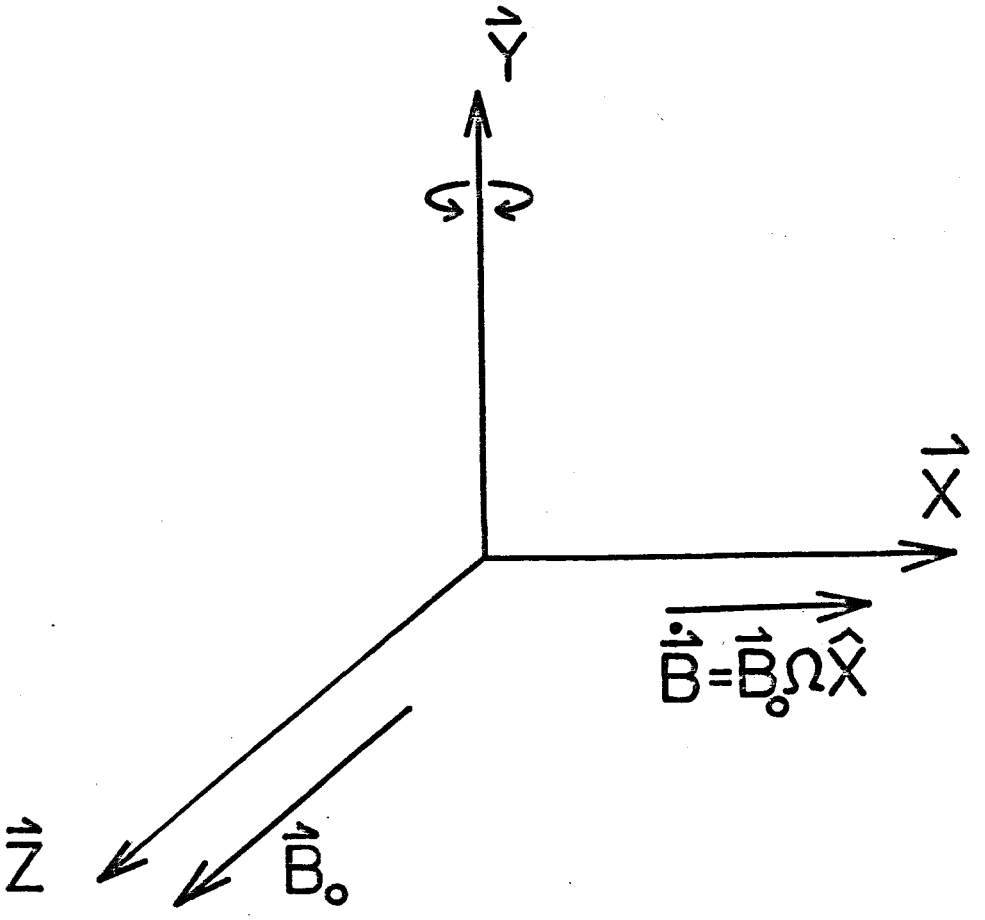

The torque varies as $B_0^2 \cos^2 \xi + K$ at high fields if an open orbit exists in a plane perpendicular to $\vec{B}_0$ and at an angle ξ from the $\hat{X}$ axis in k space. If only closed orbits are present the torque is smaller, and saturates at high fields or is linear in field.

II.2 Skin Effects and De Haas van Alphen Torques

The eddy currents induced by an oscillating magnetic field $\vec{B}$ may produce a moment $\vec{M}$ of such strength that the field at the sample core is significantly less than $\vec{B}$. The classical skin depth δ is that distance into the sample where the field is diminished by $\frac{1}{e}$ (37%). δ can be expressed (Delaney and Pippard, 1972)

$$\delta = \left(\frac{\rho}{\omega \mu_0}\right)^{1/2}$$

where ρ is the resistivity, ω the frequency of the field oscillation, and μ_0 is the permeability constant. Skin effects will be dealt with more completely in chapter 3.

At high magnetic fields ($\omega_c \tau >> 1$) de Haas van Alphen oscillations in susceptibility may occur. A strong magnetic field B_0 splits Fermi sea into discrete energy levels called Landau levels, whose energy and separation are field dependent. In k space, these levels are concentric cylindrical shells coaxial with $\vec{B}_0$. If B_0 is increased so that a Landau level moves beyond the Fermi energy, the electrons in that level must drop to lower levels. This occurs periodically in B_0^{-1}. The electron free energy (and therefore magnetic susceptibility) becomes periodic in B_0^{-1}. For more complete discussion see Gold (1968). The resistivity may

also oscillate in this way, known as the Shubnikov - de Haas effect. (Ziman, 1964). Such oscillations may be found superposed on the induced torque, and will be called de Haas van Alphen (dHvA) effects or torques in this work.

De Haas van Alphen measurements provide some information to this study, discussed in Chapter 7. More frequently, dHvA oscillations interfere with torque measurements. De Haas van Alphen torques do not change direction upon reversal of rotation direction; an induced torque does. Therefore, dHvA torques can be eliminated by recording data during rotation in opposite directions, and subtracting torques at each position. This technique was first exploited by Holroyd et al. (1975). A modification of this principle is employed in the method of position modulation, to be discussed in the next chapter.

CHAPTER 3

THE INDUCED TORQUE MAGNETOMETER

The induced torque measurements reported in Chapter 6 were not made by rotating a sample at a uniform rate. A magnetometer conceived and built by Verge et al. (1977) was used: this instrument forces the sample to oscillate angularly.

Details of the use of this magnetometer are presented in sections 1 and 2. De Haas van Alphen and static torques are shown to be minimized in section 3. Sections 4 and 5 describe modifications which should make the magnetometer simpler to use and extend its function.

An analysis of possible effects of non-uniform rotation is made in the next chapter.

III.1 Uniform Sample Rotation

The sample and its cylindrical holder are encased in a spherical rotor of moment of inertia $\sim 10^{-7}$ kgm^2. The rotor also supports sensors that allow supportive electronics to determine rotor position, and an external torque can be supplied to the rotor to reduce deviation from an electronically set reference position.

There are two modes of operation: the first uses simple rotation and the second uses rotation with position modulation.

The externally applied torque tending to bring the rotor to the reference position can be expressed

$$C(\theta(T)-\theta_D(T)) \tag{3.1a}$$

where $\theta_D(T)$ is the electronic reference position,

$\theta(T)$ is the rotor position,

and C is the reciprocal of the compliance, measured under static conditions to be $(180 \text{ radians/N-m})^{-1}$

In rotation studies where magnetic field is constant, induced torque can be expressed by

$$Ny = -b\dot{\theta} \tag{3.1b}$$

where $b = \frac{4\pi R^5}{15} B_o^2 \sigma'_{xx}$

and $\dot{\theta}$ is rotation rate

This is consistent with the results of Chapter 2. The minus sign is due to the fact that induced torque opposes rotation, by Lenz's Law.

The total force on the rotor, then, is

$$I\ddot{\theta} = -b\dot{\theta} + C(\theta-\theta_D), \tag{3.1c}$$

where I is the moment of the rotor, and $\theta,\dot{\theta},\ddot{\theta}$ are understood to be functions of time.

The reference position θ_D is supplied to the magnetometer as a voltage: similarly, angular position θ is available at some stage as a voltage, and the processing of θ depends on the mode of operation.

Uniform rotation is achieved by making θ_D linear in time, $\theta_D = ET$. Solving equation (3.1c) for θ.

$$\theta = Et + \frac{E}{C} b \tag{3.2}$$

In the uniform rotation mode the magnetometer output is a voltage proportional to $(\theta-\theta_D)$ and the induced torque is plotted by the magnetometer as a function of θ.

III.2 Angular Oscillation or Position Modulation

Position modulation is an oscillation of the sample about some equilibrium angle, forced by an externally applied torque. Typically, modulation is at a frequency of 1.5 to 10 Hz, at amplitudes up to 1.5 degrees (0.03 radians). Frequently, modulation and gross rotation are combined by moving the equilibrium position at a uniform rate, while employing modulation.

By position modulation, rotation rate (and therefore signal strength) are increased. Another benefit is dHvA signal averaging as explained in Chapter 2.

The externally applied alternating torque is realized in the following way: A reference position is provided (fed to the magnetometer as a voltage) of the form

$$\theta_D = \theta_o \cos \omega t + Et + F \tag{3.3}$$

where θ_o is modulation amplitude

ω is modulation frequency

E is gross rotation rate

F defines initial position.

A torque is applied as in (3.1a) to follow θ_D.

$$I\ddot{\theta} = -b\dot{\theta} + C[\theta-(\theta_o \cos \omega t + Et + K)] \tag{3.4}$$

Assuming a solution of the form

$$\theta = \alpha \cos \omega t + \beta \sin \omega t + et + f \tag{3.5}$$

and substituting into the differential equation (3.4), results in

$$\theta = \theta_{D_o} \frac{C(C-I\omega^2)\cos \omega t}{(C-I\omega^2)^2 + (b\omega)^2} - \frac{\theta_o \omega bC \sin \omega t}{(C-I\omega^2)^2 + (b\omega)^2} + Et + \frac{bE}{C} + F \tag{3.6}$$

The last three terms of equation (3.6) recover the simple rotation case, as in equation (3.2). The rotation rate associated with modulation is identified as $\theta_o\omega$ and $\theta_o\omega b$ is the induced torque.

The magnetometer supplies a voltage proportional to θ for signal processing. Terms of equation (3.6) constant or linear in time are eliminated from this voltage through comparison with gross rotation rate by difference amplification.

A voltage proportional to induced torque is realized through standard phase detection techniques: The voltage proportional to θ is inverted when $\cos \omega t = -1$ for one half period interval. The resultant has an average of zero contributed by any $\cos \omega t$ component: the $\sin\omega t$ component survives, and the output is proportional to the coefficient of $\sin\omega t$ in θ, denoted β in (3.5),

$$\beta = \frac{\theta_o \omega bC}{(C-I\omega^2)^2+(\omega b)^2} \tag{3.7}$$

This signal is applied to the input of a Schmitt trigger, and smoothed by RC networks. A Schmitt trigger is sensitive to amplitude, but the component $\sin \omega t$ is small compared to $\cos \omega t$, and little

amplitude mixing with phase detection is anticipated.

From the preceding discussion, the rotor is seen to be a harmonic oscillator, driven below its natural frequency. Induced torque damps the motion, much as a viscous force, lowering the natural frequency ($\sim$ 300 Hz) and lowering Q. β may not be linear in ω, in the case of large b. Since little information is obtained if β is non-linear in ω, this is checked when data is taken.

The enhancement of signal strength is significant: effective rotation rates $\theta_0\omega$ may be obtained with values up to 3.6 radians/sec. Direct rotation of 100°/minute is 0.033 radians/sec, 2 orders of magnitude less, and technically difficult to achieve. Rotation rates of 3.6 radians/sec would produce significant skin effects in good conductors, but modulation techniques are not necessary for good conductors; direct rotation measurements are sensitive enough.

Skin effects are not as severe for crystals with high resistivity, so modulation techniques are useful.

A tacit assumption has been made throughout this chapter, that departure from the direct rotation case has not changed the character of the torque N_y. The nature of perturbations arising from position modulation are presented in the next chapter.

III.3 Elimination of dHvA and Static Torques

Static torques on the rotor are an artifact of the instrument's construction, are position dependent, vary smoothly as a function of angular position, and may amount to several hundred dyne-cm. A more fundamental difficulty is due to dHvA torques.

If sampled over a sufficiently small angular range, a linear approximation is suitable for describing these unwanted torques. Upon substituting a term $g(\theta) = g\cdot\theta + f$ into the differential equation

$$I\ddot{\theta} = -b\dot{\theta} + C(\theta-\theta_D) + g\cdot\theta + f \tag{3.8}$$

Using the variational methods already employed

$$\theta(T) = \frac{C\theta_o(C-g-I\omega^2)\cos\omega t}{(C-g-I\omega^2)^2 + (b\omega)^2}$$

$$+ \frac{C\theta_o b\omega \sin\omega t}{(C-g-I\omega^2)^2 + (b\omega)^2} + \frac{CEt}{C+g} + C\,\frac{bE + F(C+g)}{(C-g)^2} \tag{3.9}$$

If g is zero, the case already solved is recovered. The value of C is 5.56×10^4 dyne cm/radian, and g may be .5% that value. Little survives the demodulation and subsequent averaging in the coefficient of sin ωt, but some part survives which is difficult to quantify.

III.4 Zero Torque

The output of the torque magnetometer system is a dc voltage proportional to the induced torque. It is difficult to establish the zero-torque level because of the phase detection technique.

The magnetometer can be operated below 0.1 T only under special conditions, so the zero of induced torque must be found by extrapolating the ω dependence of the torque to zero ω. This is difficult because at low ω the phase is difficult to set.

If a reference signal were supplied to the lockin amplifier, 90° out of phase with the position modulation voltage, the detected signal would be the useful [induced torque] signal. If such a

reference is supplied to the Princeton HR-8 lockin amplifier, no phase adjustment is necessary.

III.5 Induced torque measurement of ρ_{xy}

There are induction techniques for measuring the Hall term of the resistivity tensor ρ_{xy}, notably helicon techniques. A minor modification should allow measurement of ρ_{xy} using the torque magnetometer.

If $\dot{\vec{B}}$ were made parallel to $\hat{Y}$, the direction of the torque axis,

$$\vec{N} = \kappa \vec{B}_o \times \overleftrightarrow{\sigma}' \cdot \dot{\vec{B}} = \kappa B_o \begin{pmatrix} 0 \\ 0 \\ 1 \end{pmatrix} \times \begin{pmatrix} \sigma_{xy}' \\ \sigma_{yy}' \\ \sigma_{zy}' \end{pmatrix} = \kappa B_o \dot{B} \, (-\sigma_{yx}', \sigma_{xy}', 0) \qquad (3.10)$$

where $\kappa = \dfrac{4\pi r^5}{15}$

and $\sigma_{xy}' = \dfrac{\rho_{xy}}{(\rho_{xx}+\rho_{xz})(\rho_{xx}+\rho_{yy}) + \rho_{xy}\rho_{yx}}$

$$\simeq \frac{1}{\rho_{xy}} \quad \text{at high fields, } (\rho_{xy} >> \rho_{xx})$$

Therefore $N_y = \kappa B_o \dot{B} \, \sigma_{xy}' \simeq \dfrac{\kappa B_o \dot{B}}{\rho_{xy}}$ at high fields.

$\dot{\vec{B}}$ can be produced by a pair of Helmholtz coils attached to the torque head, but it remains to see whether N_y will be observable. For a sample of radius 1 mm, $\kappa \sim 10^{-14} m^5$.

Taking a typical figure of ρ_{xy} from Kittel (1971),

$$\sigma_{xy}' = \frac{1}{\rho_{xy}} \sim 10^{10} \, (\Omega m)^{-1} \, B_o$$

Using $B_o = 3T$, $B_o \kappa \sigma_{xy}' \sim 10^{-3} \frac{Nms}{T}$: to obtain a torque of 10^{-6} newton meters, $\dot{B}$ must be 10^{-3} tesla/sec.

Assuming a small helmholtz pair is capable of 0.5 gauss ($5 \cdot 10^{-5}$ tesla), the frequency required is $\omega = 20S^{-1}$, or 3.3 Hz.

The field amplitude 0.5 gauss is a conservative estimate, and a much stronger field is attainable despite space restrictions imposed by the size of the existing apparatus. It is important that $\vec{\dot{B}}$ be uniform over the sample.

The magnetometer response to this torque is given by

$$I\ddot{\theta} = -b\dot{\theta} + C(\theta - \theta_D) + B_o \kappa \dot{B} \sigma_{xy}' \tag{3.11}$$

$$\text{If } \dot{B} = B_y \omega \cos \omega t \tag{3.12}$$

and assuming a solution of the form

$$\theta = M \cos wt + N \sin wt + F \tag{3.13}$$

upon substituting θ into (5.10),

$$\theta = \frac{-B_o \omega B_y}{I} \kappa \sigma_{xy}' \frac{(C - I\omega^2)}{(C - I\omega^2)^2 + (\kappa B_o^2 \omega \sigma_{xx}')^2} \cos \omega t$$

$$+ \frac{\kappa^2 B_o^3 \omega \sigma_{xx}' \sigma_{xy}' B_y}{(C - I\omega^2)^2 + (\kappa B_o^2 \omega \sigma_{xx}')^2} \sin wt + \theta_o \tag{3.14}$$

Phase detection of the cos ωt term should be used. The cos ωt term is also, largely, independent of σ_{xx}'. The output should be independent of σ_{xx}' if the measured torque is linear in ω. Signal averaging should eliminate dHvA and static torque signals.

Measuring ρ_{xy} under the same conditions as σ_{xx}' may be useful in the interpretation of σ_{xx}'.

CHAPTER 4

THEORY OF POSITION MODULATION

The techniques used for solving for $\vec{N}$ in the case of uniform rotation are valid with modulation also. Critical to this is the retention of the quasistatic approximation: it is still valid, though rotation rates are two orders of magnitude greater. This leads immediately to the result $N = \kappa \vec{B}_0 \times \sigma' \cdot \dot{\vec{B}}$, equation (1.12), where κ is a constant.

A significant departure from the uniform rotation case is the time dependence of fields $\vec{B}_0$ and $\dot{\vec{B}}$. If the sample position is given by $\theta=\theta_R \cdot \cos \omega_R T$, the position of arbitrary crystal axes with respect to the applied field is

$$\vec{B}_0 = B_0[\sin(\theta_R \cos\omega_R T)\hat{X} + \cos(\theta_R \cos\omega_R T)\hat{Z}] \tag{4.1}$$

$$\dot{\vec{B}} = -B_0 \omega_R \theta_R \sin\omega_R T[\sin(\theta_R \cos\omega_R T)\hat{Z} - \cos(\theta_R \cos\omega_R T)\hat{X}] \tag{4.2}$$

The externally applied torque is, of course, finite, and N might be large enough to make the assumption of simple θ inaccurate. If a more complicated function is needed, however, it will be periodic in time and could be expressed

$$\theta = \sum_R (\theta_R \cos\omega_R T + \theta'_R \sin\omega_R T) \tag{4.3}$$

With the understanding that θ may be complicated, (1.12) is rewritten

$$N = B_o\kappa \begin{pmatrix} \sin\theta \\ 0 \\ \cos\theta \end{pmatrix} \quad X\overleftrightarrow{\sigma'} \cdot B_o\dot{\theta} \begin{pmatrix} -\cos\theta \\ 0 \\ \sin\theta \end{pmatrix} \tag{4.4}$$

A term involving σ_{zz}' is now mixed with σ_{xx}' in N. In the high field limit, for an uncompensated metal σ_{zz}' may be five orders larger than σ_{xx}'. The amplitude of θ is expected to be close to the electronically controlled reference, $\sim 10^{-2}$ radians. Expanding the expression for $\sin^2\theta$ and $\cos^2\theta$ in Taylor series would still have the term involving σ_{zz}' one order larger than the term involving σ_{xx}', in the worst case.

The differential equation governing magnetometer response (expression (3.1c)) becomes

$$I\ddot{\theta} = -\kappa B_o^2\dot{\theta}[\cos^2\theta\sigma_{xx}' - \sin^2\theta\sigma_{zz}'] + C\theta - C\theta_o \cos wt \tag{4.5}$$

It is not unreasonable to expect such a nonlinear equation in such an interactive system, as pointed out in earlier remarks on the nature of θ. This can be solved by taking approximations

$$\cos^2\theta = [1-\frac{\theta^2}{2} + \frac{\theta^4}{4!} + \ldots]^2 \sim 1-\theta^2 + [\frac{1}{4} + \frac{1}{4!}]\theta^4 \ldots \tag{4.6}$$

$$\sin^2\theta = [\theta-\frac{\theta^3}{6} + \frac{\theta^5}{5!} + \ldots]^2 \sim \theta^2-\frac{\theta^4}{3} + [\frac{1}{36} + \frac{2}{5!}]\theta^6 \ldots \tag{4.7}$$

Since θ^4 is four orders smaller than θ^2, take $\sin^2\theta\sim\theta^2$, and $\cos^2\theta\sim 1$.

Making these replacements in (4.5), and defining $\kappa' = \kappa B_o^2$,

$$I\ddot{\theta} = -\kappa\dot{\theta}(\sigma_{xx}'-\theta^2\sigma_{zz}') + C(\theta-\theta_o\cos\omega t) \tag{4.8}$$

Note that if $\sigma_{zz}' = 0$, the case treated in Chapter 3 is recovered: see equation (3.4). The term $\kappa\dot{\theta}\theta^2\sigma_{zz}'$ contains all significant perturbations introduced by modulation. Several approaches were made to find a solution, but the only success is achieved by using Laplace transforms in an iterative procedure. An approximation is made to θ using $\sigma_{zz}' = 0$: this solution is then used in θ and θ^2 to include σ_{zz}'. Finally, the effects of another iteration are examined.

For $\sigma_{zz}' = 0$, a solution is found; setting $P = \kappa\sigma_{xx}'$,

$$\theta = \frac{\theta_o C(C-I\omega^2)}{(C-I\omega^2)^2+(P\omega)^2}\cos\omega t + \frac{C\theta_o P\omega}{(C-I\omega^2)^2+(P\omega)^2}\sin\omega t$$

$$+\theta_o \exp\left(-\frac{Pt}{2I}\right)\left\{\left[\frac{\frac{P}{2}+\frac{PC^2+PC(C-I\omega^2)}{(C-I\omega^2)^2+(P\omega)^2}}{\left(\frac{C}{I}-\frac{P^2}{4I}\right)^{\frac{1}{2}}}\right]\sin\left(\left(\frac{C}{I}-\frac{P^2}{4I}\right)^{\frac{1}{2}}t\right)\right.$$

$$\left.+\left[1+\frac{C(C-I\omega^2)}{(C-I\omega^2)^2+(P\omega)^2}\right]\cos\left(\left(\frac{C}{I}-\frac{P^2}{4I}\right)^{\frac{1}{2}}t\right)\right\} \tag{4.9}$$

If $P \neq 0$, as it must be, after some time θ damps to

$$\theta = \frac{(C-I\omega^2)\theta_o}{(C-I\omega^2)^2+(P\omega)^2}\cos\omega t + \frac{\theta_o\omega P\,C}{(C-I\omega^2)^2+(P\omega)^2}\sin\omega t \tag{4.10}$$

$$\theta \sim \theta_o \cos \omega t + \frac{(\kappa'\sigma_{xx}'\omega)}{c} \theta_o \sin \omega t \tag{4.11}$$

which has been found previously.

The term $\dot{\theta}\theta^2\kappa'\sigma_{zz}'$ has terms such as $\sin^3 \omega t$. These are reduced using trigonometric identities to simple functions

$$\dot{\theta}\theta^2 = a_1 \cos\omega t + b_1 \sin\omega t + a_3 \cos 3\omega t + b_3 \sin 3\omega t \tag{4.12}$$

The coefficients are functions of the coefficients found in (4.11). Including the terms of (4.12) in (4.8), the system is solved again, by the same method. Equation (4.11) is recovered, with new terms as well

$$\theta = \{\theta_o + \frac{\theta_o^3(\kappa'\sigma_{xx}'\omega)(\kappa'\sigma_{zz}'\omega)}{c^2}\} \cos \omega t$$
$$+ \frac{\kappa'\sigma_{xx}'\omega)\theta_o}{c} + \frac{\theta_o^3(\kappa'\sigma_{zz}'\omega)}{4c} \left(1 - \overbrace{\frac{(\theta_o\kappa'\omega\sigma_{xx}')^2}{c^2}}^{a}\right) \sin \omega t$$
$$+ \frac{\theta_o^3(\kappa'\sigma_{zz}'\omega)}{c} \{\cos (3\omega t) + \sin (3\omega t)\} \tag{4.13}$$

Note that term a is very small compared to one. Terms decaying in time have not been included.

Reiteration will produce a closer approximation to θ. The terms in frequency 3ω will produce terms of still higher frequencies (with smaller coefficients) which will be filtered out by the lockin amplifier. Eliminating term a, terms in 3ω and approximating the coefficient of $\cos\omega t$ to be θ_o

$$\theta = \theta_o \cos\omega t + \frac{\theta_o\kappa'\omega}{c} (\sigma_{xx}' + \frac{\theta_o^2}{4} \sigma_{zz}') \sin\omega t \tag{4.14}$$

Given $\rho_{xy} >> \rho_{xx}$, then $\sigma_{zz}'/\sigma_{xx}' \sim \rho_{xy}^2/\rho_{xx}^2$. This ratio must be small to assure that only σ_{xx}' is measured. A worst case would be aluminum: at 1T $\rho_{xx} \sim 9 \cdot 10^{-12}$ Ωm (Delaney and Pippard 1972: Balcombe et al. 1964) and $\rho_{xy} \sim 10^{-10}$ Ω (Goodman, 1968). In this case $\sigma_{zz}'/\sigma_{xx}' \simeq 120$. The value of $\theta_o^2/4$ is $2.5 \cdot 10^{-5}$ ($\theta_o = 0.01$) and the induced torque is changed by only 0.3%. The magnetoresistance of Al is small, however at higher fields $\sigma_{zz}'/\sigma_{xx}'$ is increased somewhat by the field dependence of ρ_{xy}^2: as much as 5% of the total torque may be due to σ_{zz}' at 8.5 T. Clearly, systematic error can occur: it can be monitored, however, by monitoring torque linearity in θ_o.

Because of the product $\kappa'\sigma_{zz}'\dot{\theta}\theta^2$ in the differential equation (4.8), the next iteration will replace σ_{xx}' by $(\sigma_{xx}' + \theta_o^2 \sigma_{zz}'/4)$ in term a of (4.13). Term a can still be neglected, and successive reiteration does not change this situation: equation (4.14) is a very good approximation.

In conclusion, systematic errors introduced by position modulation are of order 5% in the worst case of a very high purity metal at high fields, with no open orbits perpendicular to the magnetic field. In the case of $Hg_{3-\delta}AsF_6$, ρ_{xx} is much higher than in the test case and no problems are anticipated. If the magnetometer is used with very good metals, the effect of position modulation may be examined by monitoring the torque amplitude as a function of θ_o: any nonlinearity can probably be corrected by reducing θ_o.

CHAPTER 5

SAMPLE HANDLING AND EXPERIMENTAL CONDITIONS

$Hg_{3-\delta}AsF_6$ samples were prepared by Duane Chartier in a pyrex reaction vessel as in Figure (5.1). Hg and liquid SO_2 were frozen into the vessel using liquid nitrogen as a coolant. Gaseous AsF_5 was added, condensing onto the solid SO_2. The vessel was sealed and warmed to $\sim$ -10°C: at this temperature SO_2 is a liquid and AsF_5 goes into solution and can react with Hg. The area of the Hg surface is limited by the reaction vessel to $\sim$ 1 mm^2 in order to limit the number of nucleation sites. After crystal growth, unreacted reagents are transferred into auxilliary arms of the vessel and sealed off.

$Hg_{3-\delta}AsF_6$ is extremely hygroscopic: a few ppm of water in the atmosphere damages the surface in minutes, dulling the lustre and changing the colour from gold to grey green. Continued exposure results in the visible extrusion of Hg in such proportions that it is visible as droplets on the surface. Finally, the crystal turns black.

Induced torque is a bulk effect, and light surface damage is not critical to studies of common metals. However, the mercury extrusion accompanying damage to $Hg_{3-\delta}AsF_6$ may have a large effect on conductivity, and surface-damaged crystals were discarded. Such damage could be identified by visual examination prior to and after any experiment.

FIGURE 5.1: The reaction vessel. The portion that is not shown has an arm into which unconsumed reactants are poured, which is then sealed by standard glassblowing techniques.

FIGURE 5.2: The sample mount and rotor geometry. The rotor holds the sample holder by means of a set screw which allows the angle ϕ to be changed during the experiment. This is accomplished by means of a stainless steel screwdriver fitted to a slot in the end of the sample holder, controlled manually from outside the Dewar.

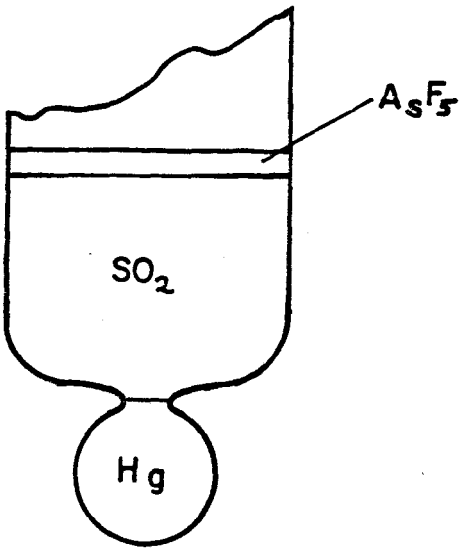
A_sF_5
SO_2
Hg

FIG. (5.1)

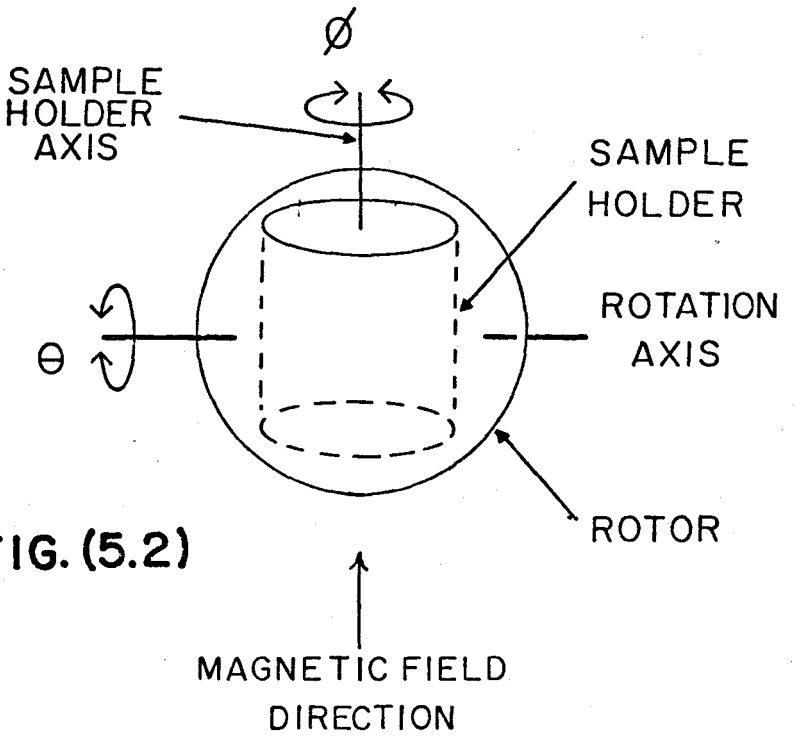
Ø
SAMPLE HOLDER AXIS
SAMPLE HOLDER
ROTATION AXIS
Θ
ROTOR
MAGNETIC FIELD DIRECTION

FIG. (5.2)

The samples were mounted in the rotor by first encasing them in sealed sample holders. The transfer from sealed reaction vessel to sample holder was done in a glove box containing a nitrogen atmosphere with less than 10 ppm of water. The sample holders were cylindrical cans 9.5 mm long and 6.4 mm in diameter, made of a clear plastic (Kel-F).

A holder with a screw cap and a neophrene plug for a seal was too delicate for repeated use. The final design used a short Kel-F plug for a seal, carefully machined to a very tight forced fit. The contacting surfaces of the plug and holder were made very smooth to ensure a good seal. No sealant [such as vacuum grease] was used since none have been found that could be dried sufficiently. The samples were held in place by tightly wadded dried Teflon tape. The seam of plugged holders was sometimes coated with an acetone based cement (glyptal). Usually the holders were mounted in the rotor and cooled to 77 K as quickly as possible: a sample might be protected from the atmosphere by the holder only for 10 to 30 minutes. The samples could be visually inspected for surface damage if mounting was delayed: one sample was left in the holder for several months with no apparent damage.

The sample holders and plugs were cleaned by a 48-hour bath in agitated nitric acid, followed by a washing with distilled water and acetone. The pieces were then placed in a clean dessicator and pumped to 10^{-5} Torr for 24 hours to outgas water. The Kel-F pieces and Teflon tape were fluorinated to eliminate any remaining water or

organic materials. The growth vessel was also fluorinated in this way: this process does not flush or remove impurities bodily, but such impurities are rendered chemically inert.

Handling problems precluded attempts to orient the samples by X-ray or neutron diffraction. Samples 1 and 2 were mounted with the $\vec{c}$ direction skew to the sample holder axis. This was done visually: the ab plane could be identified by the lustre, which is greatest for this plane.

Also, the morphology of $Hg_{3-\delta}AsF_6$ is that the ab plane is usually flat. In the case of sample 3, a flat was machined in the bottom of the interior of the sample holder. In this way sample 3 was mounted with $\vec{c}$ within 5° of the holder axis. The samples were chosen as nearly spherical as practical; most were best approximated by rectangular solids, 1-3 mm on a side.

Electrical and mechanical details of the magnetometer are discussed by Verge et al., (1977). The angle θ is used to describe rotor position. The angle ϕ specifies the position of the sample holder within (relative to) the rotor, as shown in Figure (5.2). The angle θ was changed by varying the electronic reference, as discussed in Chapter 3; ϕ was changed during an experiment by using a long stainless steel screwdriver.

The magnetic field was supplied by a NbTi superconducting solenoid. The maximum field attainable was 8.5 T. The magnetic field range for this work was 0.1 T and 8.5 T. The sample temperature was between 1.1 and 1.3 K.

CHAPTER 6

EXPERIMENTAL RESULTS

Figure (6.1) shows the induced torque N produced by a sample of $Hg_{3-\delta}AsF_6$ as a function of rotation angle θ at several values of applied field B_o. The orientation was unknown. A single peak predominates at θ=38° for all fields B_o above 2.0 T, and smaller peaks are observed at fields above 3.0 T at other positions. At $\theta \sim -50°$ there is a minimum in the induced torque reaching only 5 to 7% of the peak amplitude (38°) at 8.5 T.

A log-log plot of the field dependence of the amplitude of the major peak is linear, indicating a power law dependence. The amplitude of the major peak is proportional to $B_o^{2.14\pm.05}$ between 3.0 and 8.5 T. This is confirmed using another sample, between 1.6 and 8.5 T, figure (6.2).

At -50°, the torque is linear in B_o, confirmed using another sample between 2.0 and 8.5 T, figure (6.3). In each case the torque minimum is 90° from the position of the major peak.

De Haas van Alphen oscillations were observed in the torque output when position modulation was not used. The oscillations varied in strength from less than 10^{-7} N-m [negligible] to 10^{-5} N-m, peak to peak. In all cases, one dominant dHvA oscillation was observed, corresponding to the cross section of one portion of the Fermi surface. In some cases, beating was observed, and two cross sections could be calculated. Typical dHvA signals are shown in figure 6.4a, and a typical

FIGURE 6.1: Induced Torque of $Hg_{3-\delta}AsF_6$ as a function of rotor position. Note the major peak (38°) and the minimum in induced torque 90° away. The smaller peaks are not visible at 2.0 T. Between -25° and -75°, the torque at 4.5 T and 5.5 T are indistinguishable. Position modulation was used with amplitude 1.3° p-p and frequency 2 Hz.

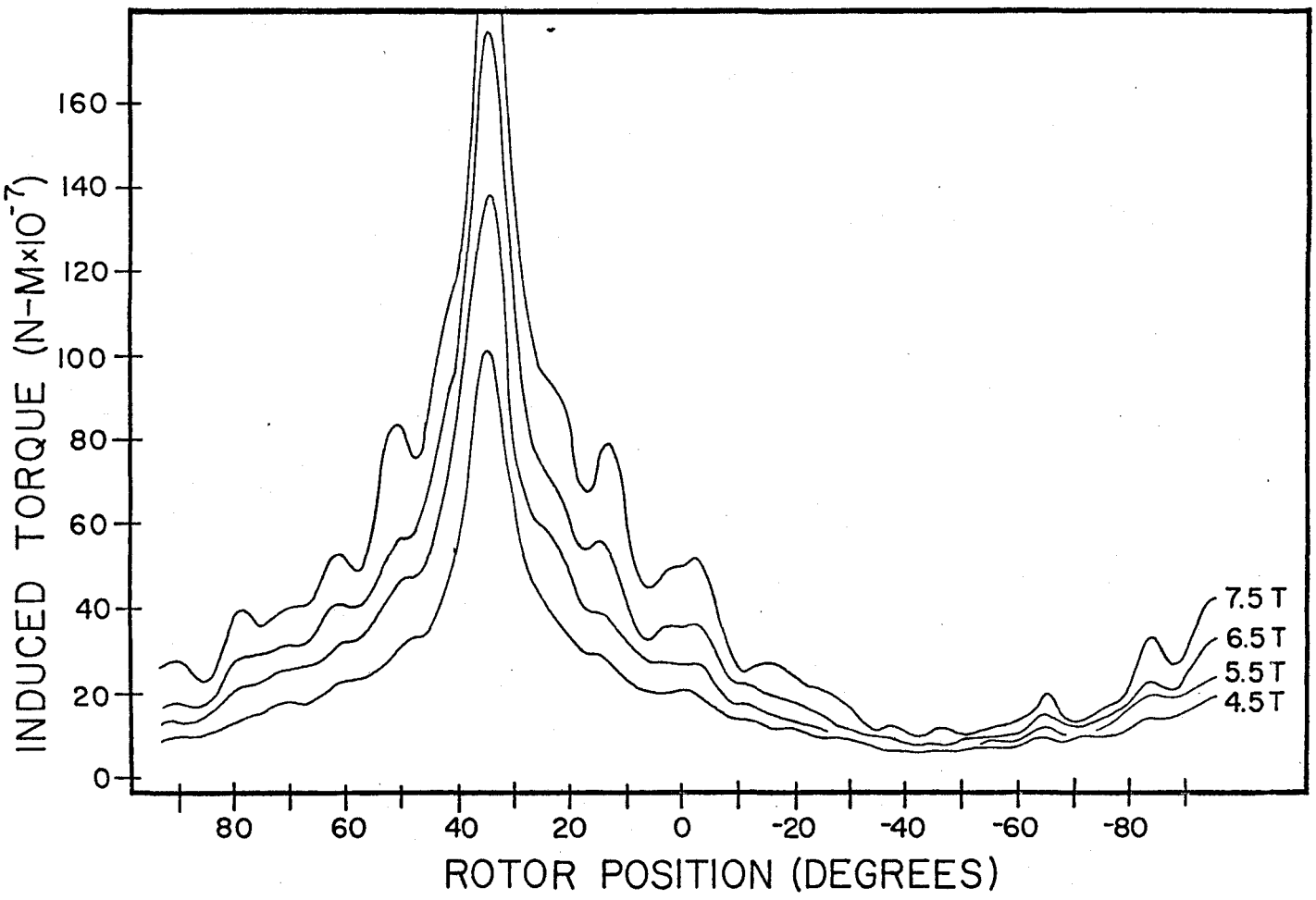
INDUCED TORQUE (N-M×10⁻⁷)
160
140
120
100
80
60
40
20
0
80
60
40
20
0
-20
-40
-60
-80
ROTOR POSITION (DEGREES)
7.5 T
6.5 T
5.5 T
4.5 T

FIGURE 6.2: Log-log plots of amplitude of the major peak versus applied field B_o. The points grouped about line A were obtained under the same conditions as rotation diagram (6.1). Here the angle θ was held constant at 37.6° (points represented by an X) and at 38.3° (dots) while the field B_o was changed. Position modulation was used, at 2 Hz and 1.3° amplitude.

Points on line C were obtained using a different sample. Position modulation at 3 Hz and 0.8° amplitude was used, with a slow angular scan (3.5° per minute) across the major peak as field B_o changed. This was done in order to minimize errors that might be due to the use of an angular position that is not at the torque peak.

The slope of each line shows the torque at the major peak is proportional to $B_o^{2.14 \pm .05}$. The slight upward deviation above 7.5 T may be due to convolution between the major peak and a rapidly growing subsidiary peak.

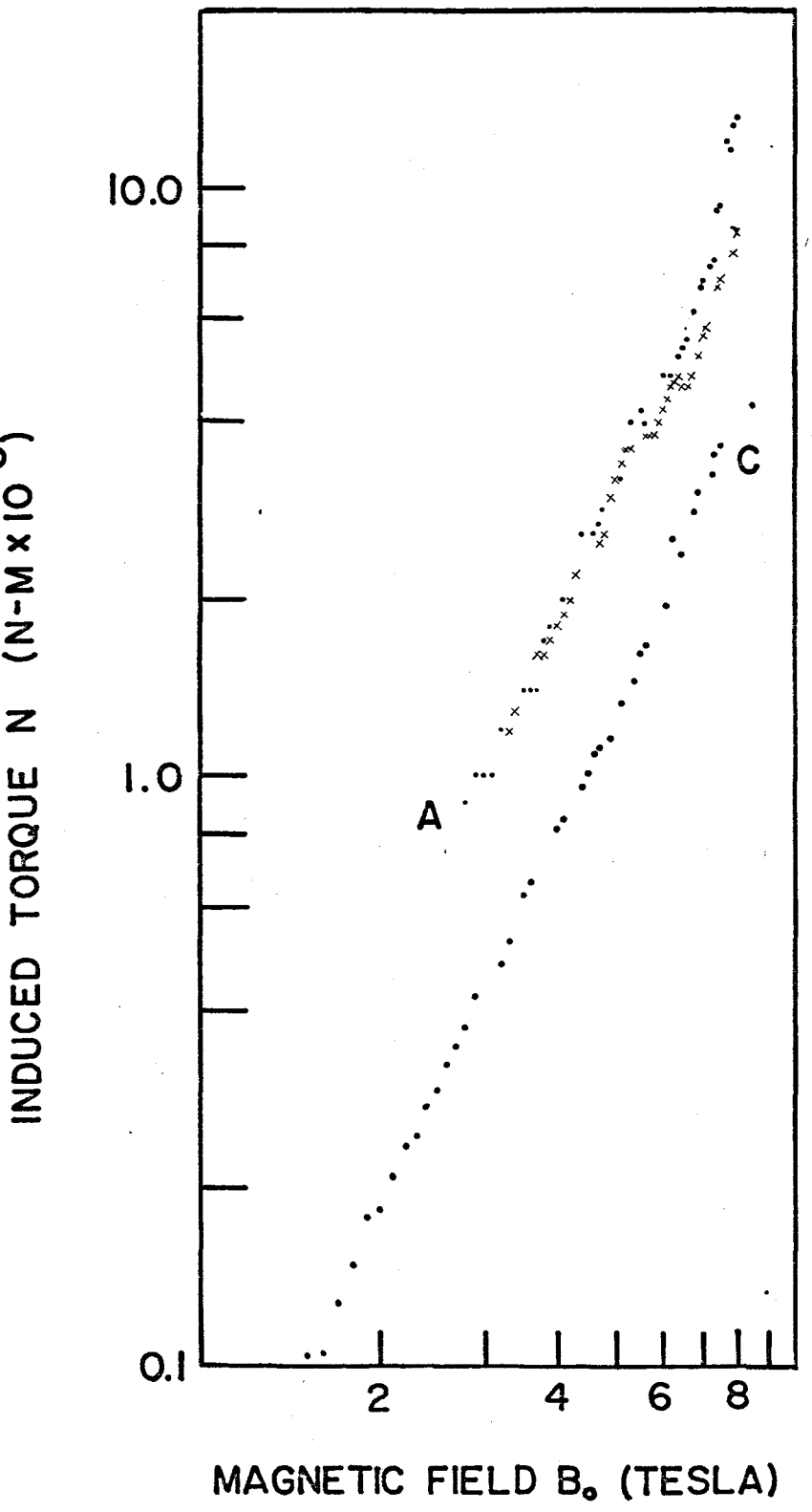
10.0
1.0
0.1
2
4
6
8
A
C
INDUCED TORQUE N (N-M x 10^-5)
MAGNETIC FIELD B₀ (TESLA)

FIGURE 6.3: Induced torque vs Applied Magnetic field at torque minima.

(a) The points referred to scale a show the induced torque of $Hg_{3-\delta}AsF_6$, taken from the rotation diagrams in figure (6.1). The torque is two orders less than at the major peak at 8.5 T.

The points referred to scale b were obtained using sample 2, position modulation frequency 3 Hz, amplitude 0.8° p-p. The zero in induced torque was obtained from data generating line c, figure (6.2) therefore very well known. The probability of no linear correlation is 0.28%.

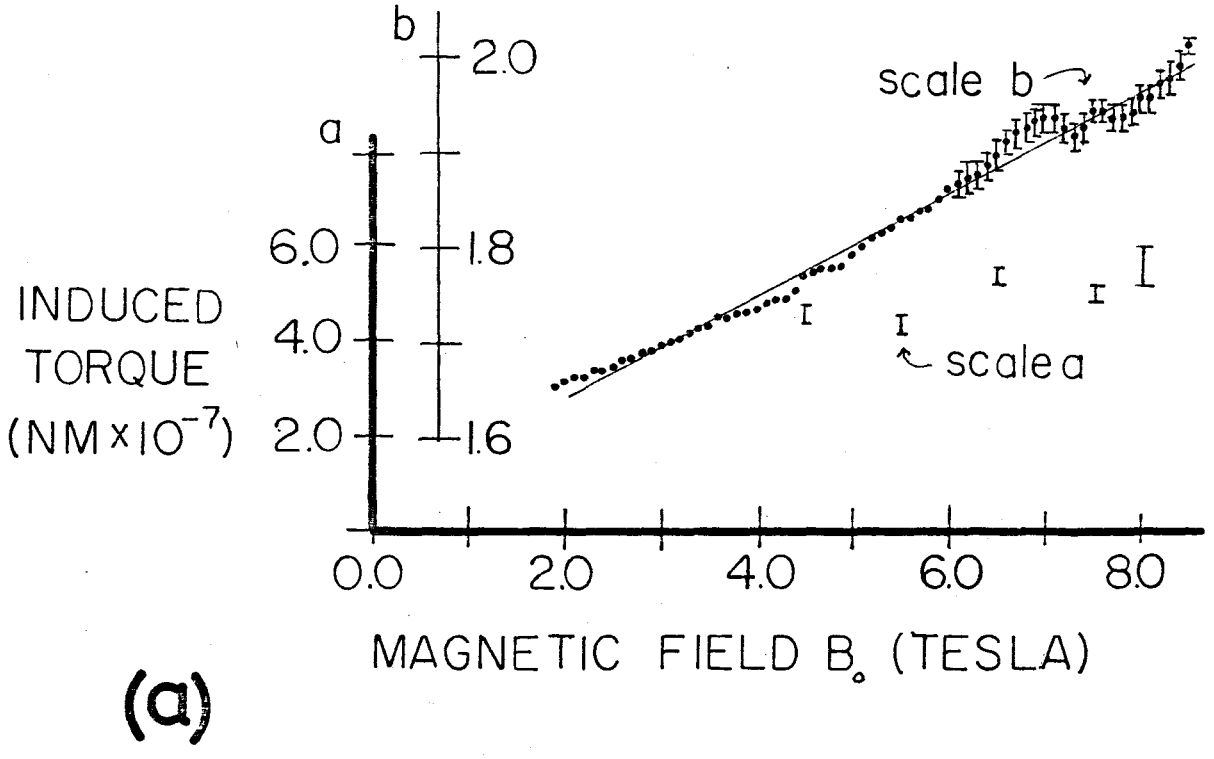

(b) The graph is a real size reproduction of the induced torque vs B_0 obtained using sample 1 at rotor position $\theta = 0°$. The modulation amplitude is 2.5° p-p at 2 Hz. The induced torque appears to be saturating, or linear, above 0.06 T. The subsidiary peak at 0° (figure 6.1) is not present at 2.0 T or below. It is an artifact of the magnetometer that measurements below 0.2 T are possible only at 0°. Above 0.2 T the random error is expected to be of the order of the trace width based on trace reproducibility. At .01 T the error is expected to be ±50%, increasing to at least 100% at zero field. The dashed lines border the area where the data is untrustworthy.

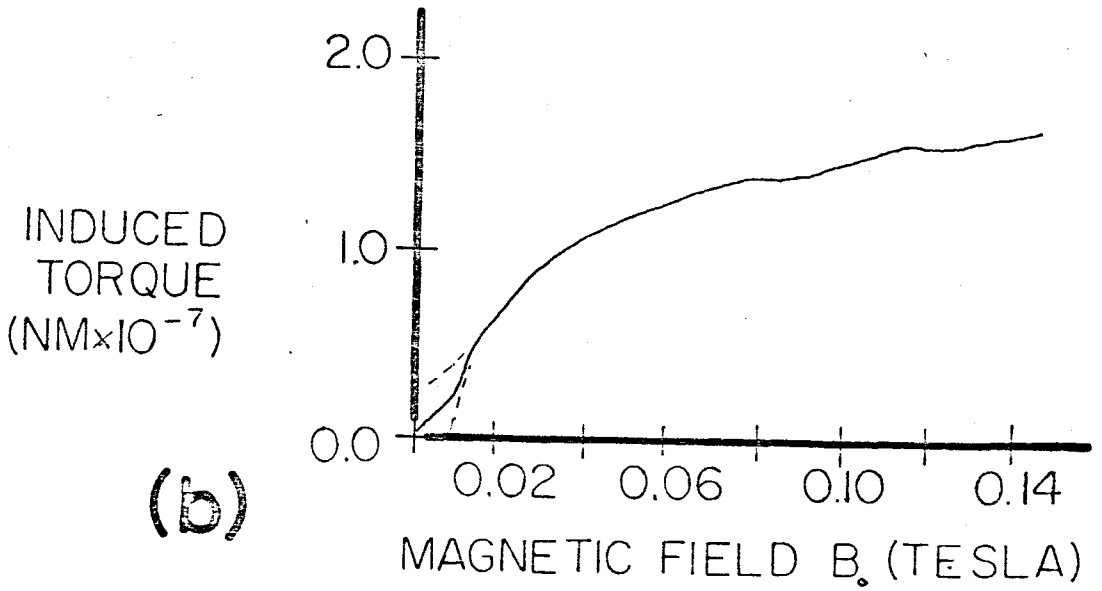

FIGURE 6.4a(i): A typical dHvA torque signal of $Hg_{3-\delta}AsF_6$ as a function of rotation angle, reduced by a factor 6. Note the beating: this indicates two dhvA frequencies are present.

FIGURE 6.4a(ii): A real size reproduction of the torque signal of Fig. 6.4a(i) between -20° and -10°. The dotted portion has an amplitude only slightly larger than the linewidth and could not be faithfully reproduced here. The upper and lower series' of dots indicate signal amplitude. The dots in the upper line mark peak positions.

FIGURE 6.4a(iii): A dHvA torque signal as a function of field, with sample stationary, 75% of actual size. The small oscillations superposed on the large oscillations are only noise.

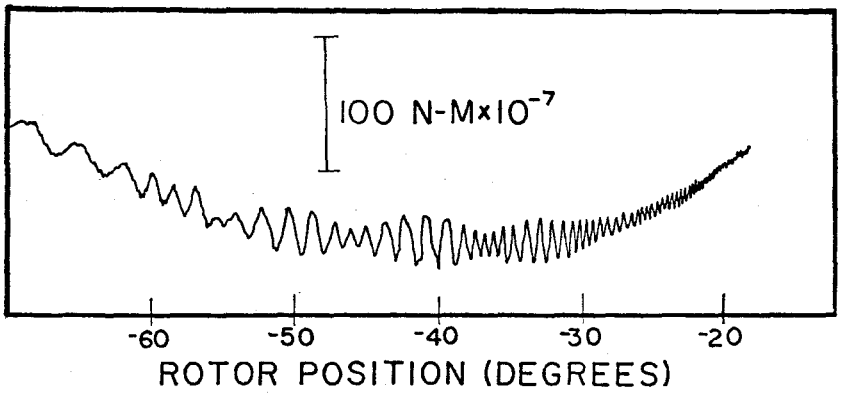

Fig. 6.4a(i)

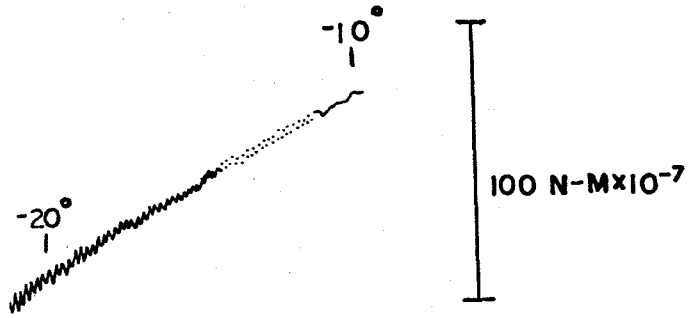

Fig. 6.4a(ii)

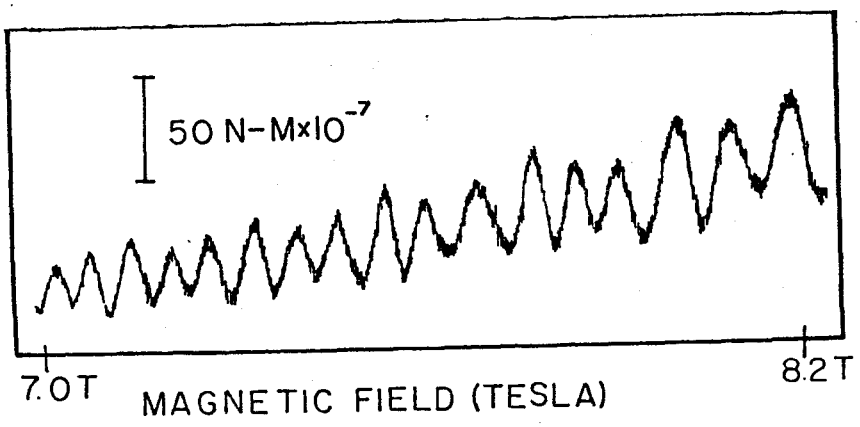

Fig. 6.4a(iii)

Fermi surface cross sectional area [perpendicular to $\vec{B}_o$] is shown in figure 6.4b. The sec θ dependence is characteristic of a cylindrical Fermi surface. DHvA torques were regularly recorded with the usual induced torque rotation diagrams.

Sample 2 was also mounted in an arbitrary way: the modulation angle was made small to allow resolution of the subsidiary peaks, figure 6.5a. Such peaks increase very rapidly with B_o above 4.5 T.A log-log plot of torque and field (figure 6.5b) shows the field dependence to be non-linear and concave upward: the torque rises more quickly than a power law B_o^n. Using a least squares fit adapted to log-log plots, values of slope [corresponding to n in $N = \kappa\sigma_{xx}' B_o^n$] range from 1.13 ± 0.78 to 17.9 ± 1.3 for fields 6.5 to 8.5 T. There are 10 subsidiary peaks: only two have n less than 2. In these cases, if data below 6.5 T is included, n is found to be greater than 2.

The orientation of the secondary peaks was obtained using a third sample mounted with the [001] direction parallel to the sample holder axis: peak positions were mapped as $\vec{B}_o$ was systematically varied to cover a solid angle of 2π steradians relative to the sample (figure 6.6). This was done by sweeping θ from -95° to +95° for settings of ϕ at 10° intervals, giving a family of rotation diagrams at different angles ϕ. This was carried out at 8.5 T to maximize signal strength. Position modulation was done at a frequency of 2 or 3 Hz and an amplitude of 0.5°, which is compatible with linear behaviour of torque amplitude in modulation amplitude and frequency.

FIGURE 6.4b: A typical Fermi Surface Cross section vs rotor position. An absolute value of Fermi surface extremal area perpendicular to $\vec{B}_o$ is found by sweeping B_o: dHvA oscillations occur in the torque required to maintain constant position θ. This was done at -82°, an error bar is shown on that point. The change in Fermi surface area as θ is varied is found using oscillations via the torque required to sweep θ with B_o fixed. The error is small compared to the error in the area at -82°. The curve is described by $A_o \sec(\theta-\theta_o)$.

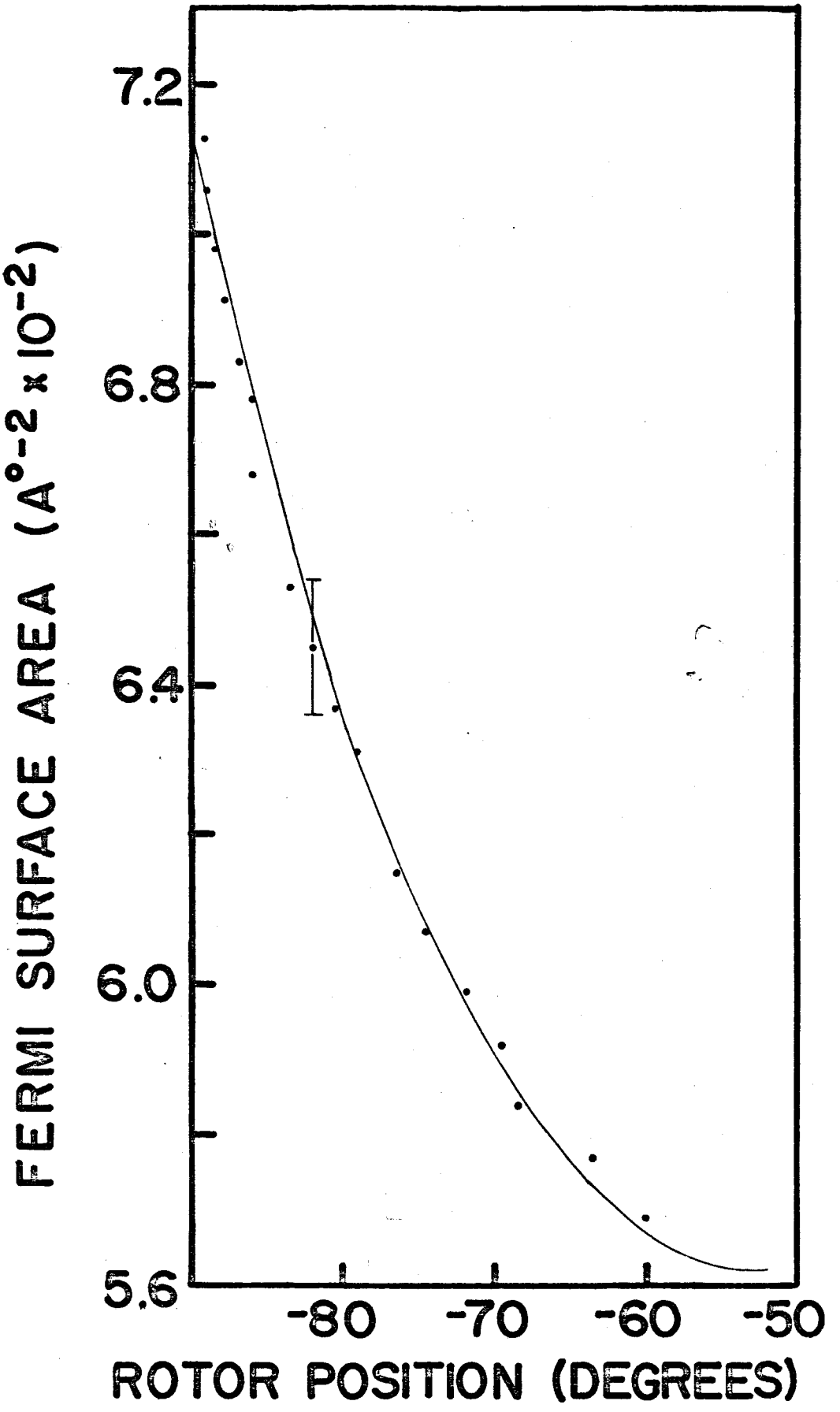
FERMI SURFACE AREA ($A^{\circ -2} \times 10^{-2}$)
7.2
6.8
6.4
6.0
5.6
-80
-70
-60
-50
ROTOR POSITION (DEGREES)

FIGURE 6.5a: Induced torque of $Hg_{3-\delta}AsF_6$ as a function of rotation angle θ (rotor position). The peaks in figure (6.1) are better resolved. Position modulation amplitude was 0.2° at 15 Hz. The rapid oscillation near -40° is an artifact of the instrument. The vertical positioning of these patterns is arbitrary: the zero-torque position is not shown.

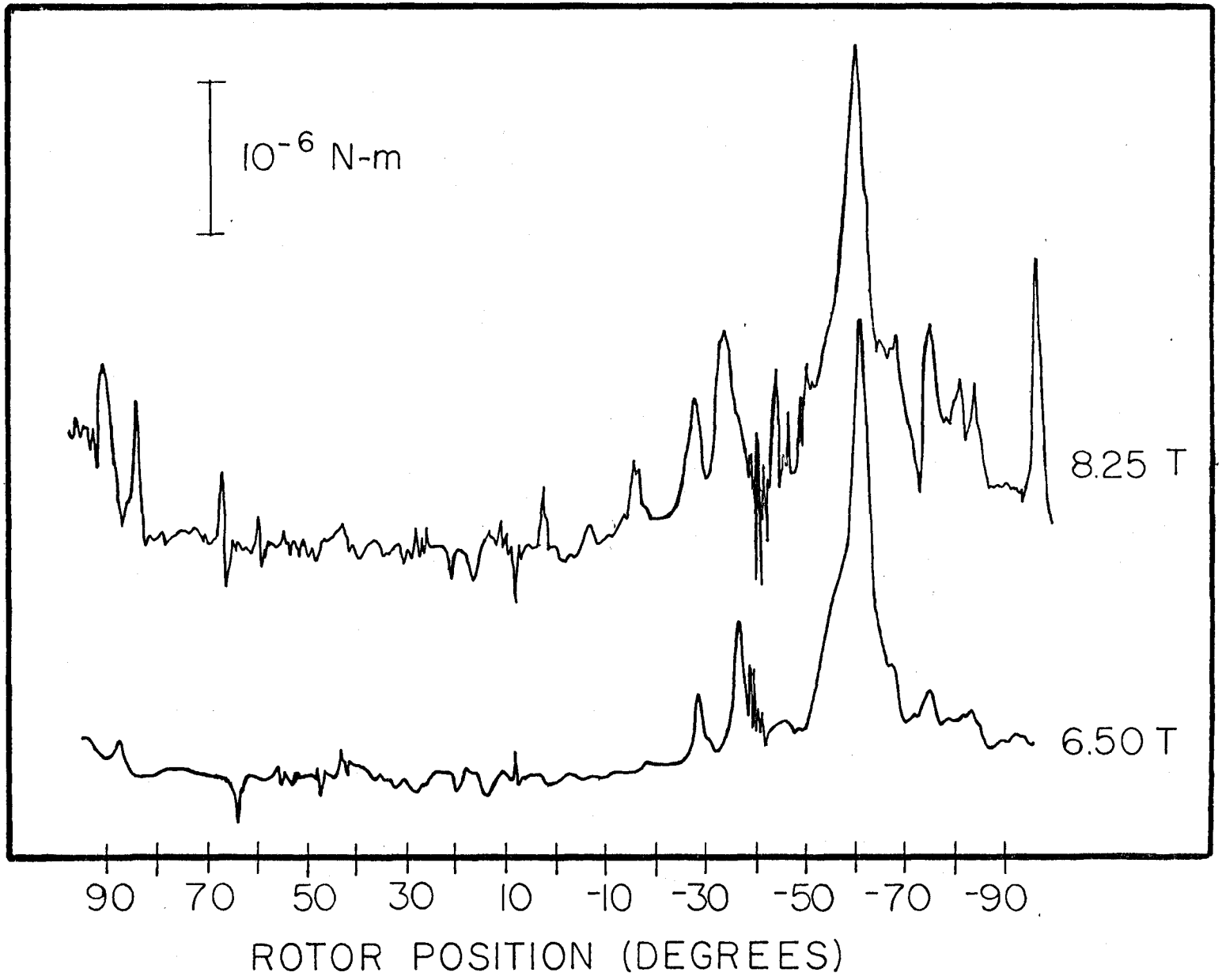
10^{-6} N-m
8.25 T
6.50 T
90 70 50 30 10 -10 -30 -50 -70 -90
ROTOR POSITION (DEGREES)

FIGURE 6.5b: Subsidiary peak amplitude as a function of magnetic field. The peak amplitudes were taken from rotation diagrams (figure 6.5a and others). The points drawn as open circles correspond to the peak at -75°, solid circles to the peak at -85°, and those marked x to the peak at -95°. The dashed curves are a guide to the eye: the line labelled D shows a B_0^2 dependence. The zero in induced torque was taken from a low field measurement at 30°. Error bars on the points marked x are correct for the other points as well, at equivalent torque levels. Data is shown for only 3 peaks for clarity. The graph shows that the peak amplitudes have a stronger than B_0^2 depence.

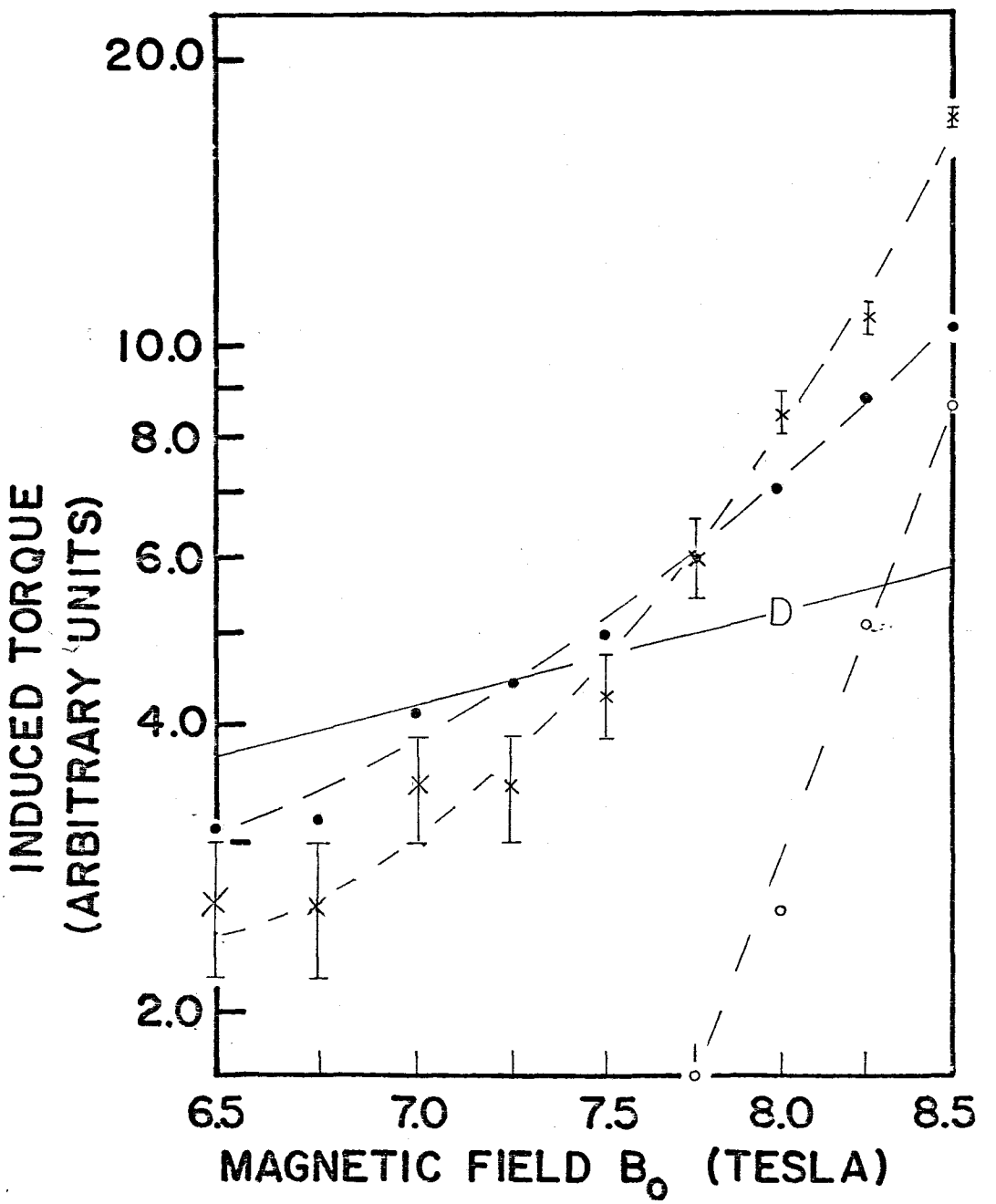
20.0
10.0
8.0
6.0
4.0
2.0
INDUCED TORQUE
(ARBITRARY UNITS)
D
6.5
7.0
7.5
8.0
8.5
MAGNETIC FIELD B_o (TESLA)

FIGURE 6.6: A stereographic projection of magnetic field directions at which peaks in the induced torque of $Hg_{3-\delta}AsF_6$ are found. Major peaks are observed if $\vec{B}$ lies in the (001) plane: this is used as a reference in mapping $\vec{B}$ directions where subsidiary peaks are found. These directions are grouped in crystallographic planes of the form (nom). Open orbits do not occur at all directions of $\vec{B}$ within such planes because magnetic breakdown is not favoured in all directions. The plot has been made with the angles between planes twice their actual size for clarity. The uncertainty in position is approximately $\pm 1^{o}$. The two symbols ($\cdot$ +) distinguish between peaks found at positive and negative θ.

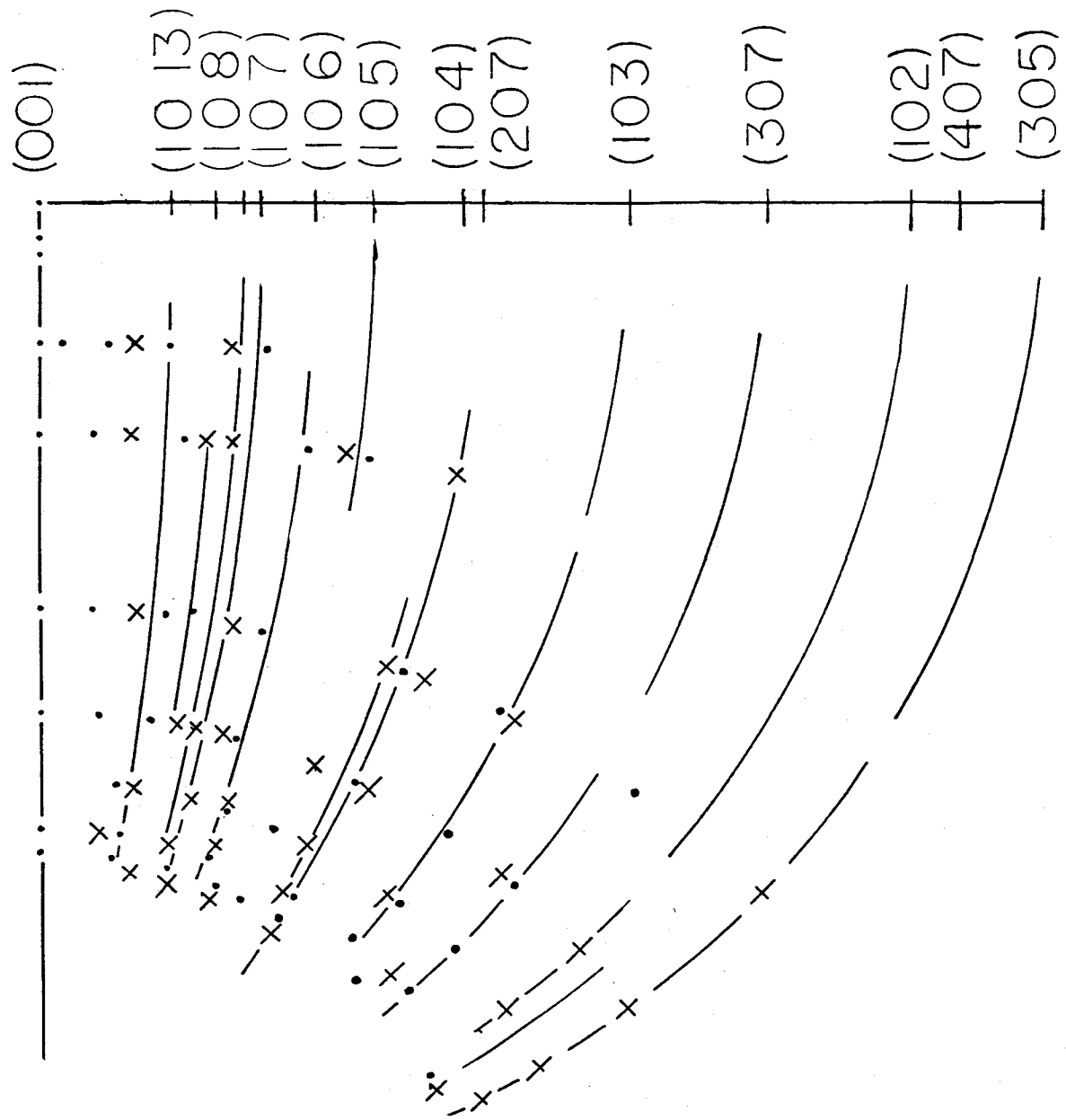
(001)
(10 13)
(10 8)
(10 7)
(10 6)
(10 5)
(10 4)
(20 7)
(10 3)
(30 7)
(10 2)
(40 7)
(30 5)

A typical rotation diagram is shown in figure (6.7) with high resolution in θ. A particularly narrow induced torque peak was observed with no subsidiary peaks, shown in figure (6.8). Since this was observed in only one crystallographic plane, it must be a symmetry plane and could be either a (100) or a (110) plane. In this case, beating of the dHvA oscillations was observed, which allows two dHvA frequencies to be obtained. At 90° from the major peaks' position, the frequencies are 604 ± 10 T and 1032 ± 14 T. If ϕ is changed by 4°, again no subsidiary peaks are found, and the dHuA frequencies are 360 ± 8 T and 724 ± 12 T.

FIGURE 6.7: A typical rotation diagram: induced torque of $Hg_{3-\delta}AsF_6$ as a function of angle θ, at constant ϕ. The rotation rate was 20° per minute, with a modulation amplitude of 0.5°. Note the dHvA oscillations between [50°,80°] and [-40°,-75°]. The dHvA oscillations appear because modulation amplitude and the whole-system time constant were kept low to avoid artificial broadening of the torque peaks. This is one of the rotation diagrams used in constructing figure (6.6). It differs from figure (6.1) in angular resolution and sample orientation, as noted in the text.

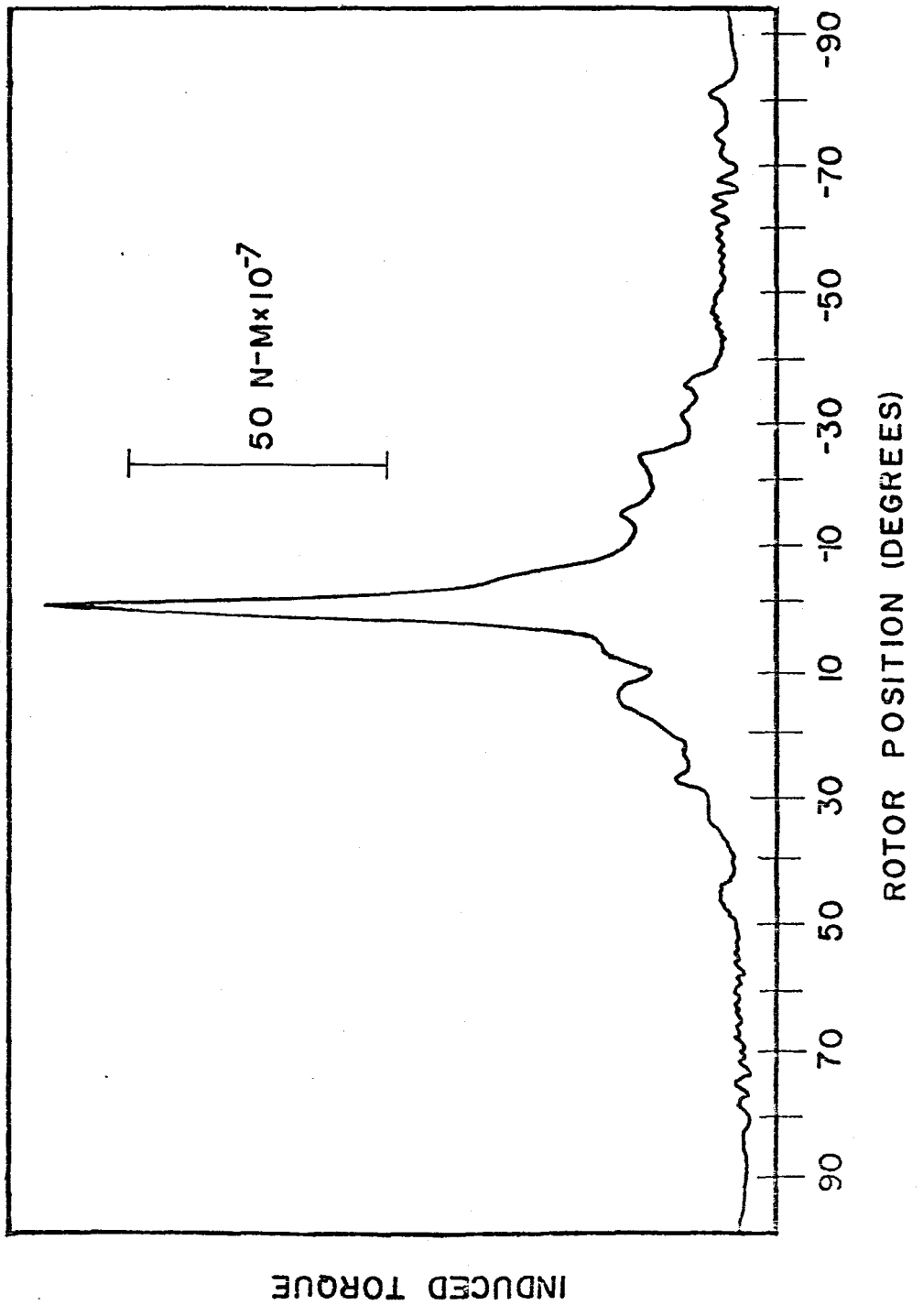
INDUCED TORQUE
50 N-M x 10⁻⁷
-90
-70
-50
-30
-10
10
30
50
70
90
ROTOR POSITION (DEGREES)

FIGURE 6.8: Induced torque of $Hg_{3-\delta}AsF_6$ as a function of angle of rotation. Note that there are no peaks due to magnetic breakdown. The background is noisy, but bears no resemblance to the magnetic breakdown peaks seen at other positions ϕ. The inset is the same peak at higher resolution. This peak was recorded with modulation amplitude and frequency of 0.25 degrees and 6.0 Hz. The rotation rate was 10° per minute: the small lines are 10° apart. The full width at half maximum was found to be 0.8°. The peak strength under these conditions (which maximize the resolution of the instrument) was 1.6×10^{-6} Nm above the background. The subsidiary peaks found in figure (6.7) are no longer present because the sample is rotated in the (100) or (110) plane.

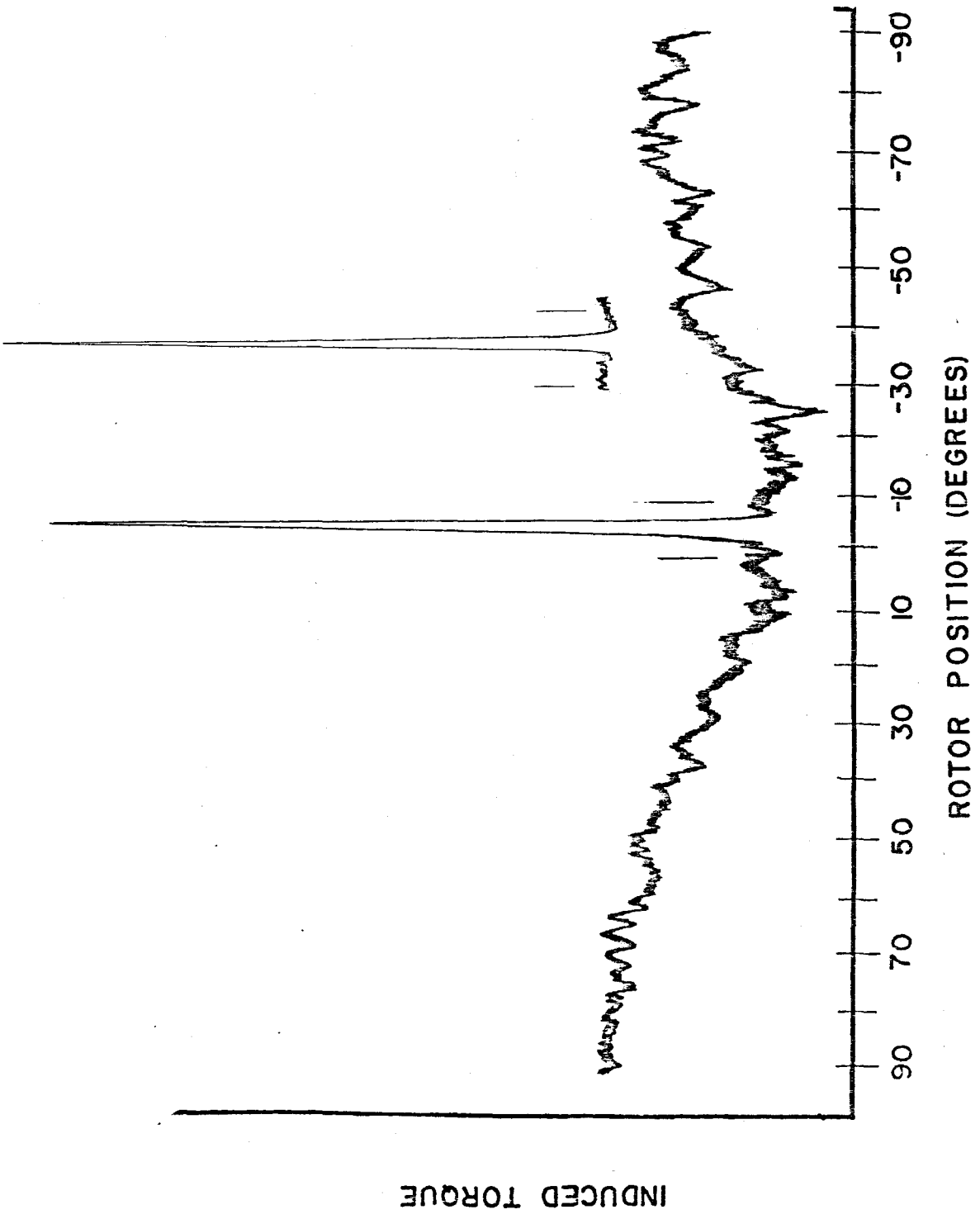
INDUCED TORQUE
90
70
50
30
10
-10
-30
-50
-70
-90
ROTOR POSITION (DEGREES)

CHAPTER 7

DISCUSSION

$Hg_{3-\delta}AsF_6$ consists of octahedral AsF_6^- ions in a body centered tetragonal lattice and chains of Hg atoms (Brown et al., 1974). The symmetry group is $I4_1/amd$: crystal parameters of the tetragonal lattice are a = b = 7.54 Å and c = 12.32 Å at room temperature. Hg chains lie in planes c/4 apart, normal to the [001] direction. Within such planes, all chains are parallel to [100] or [010]: the chains of nearest neighbouring planes alternate in direction as shown in figure (7.1). The distance between nearest parallel chains in one plane is a (7.54 Å), and the distance between Hg atoms on one chain is 2.64 Å (at room temperature).

These distances are such that no short range translation brings the lattice into itself: the AsF_6- and Hg structures are incommensurate. Crystal parameters were measured by Pouget et al. (1978) at 10 K and are listed in Table (7.1).

Adopting a suggestion by Berlinsky (1978), Razavi et al. (1979) derived a Fermi surface by treating conduction electrons as localized on Hg chains and regarding the periodicity along the chains as a perturbation. Ignoring the perturbation, the Hg chains have the symmetry elements of the AsF_6^- lattice and a Brillioun zone can be constructed. Localizing conduction electrons also means conduction along [100] and [010] directions only: the Fermi surfaces are then flat and perpendicular to (100) and (010) planes in reciprocal

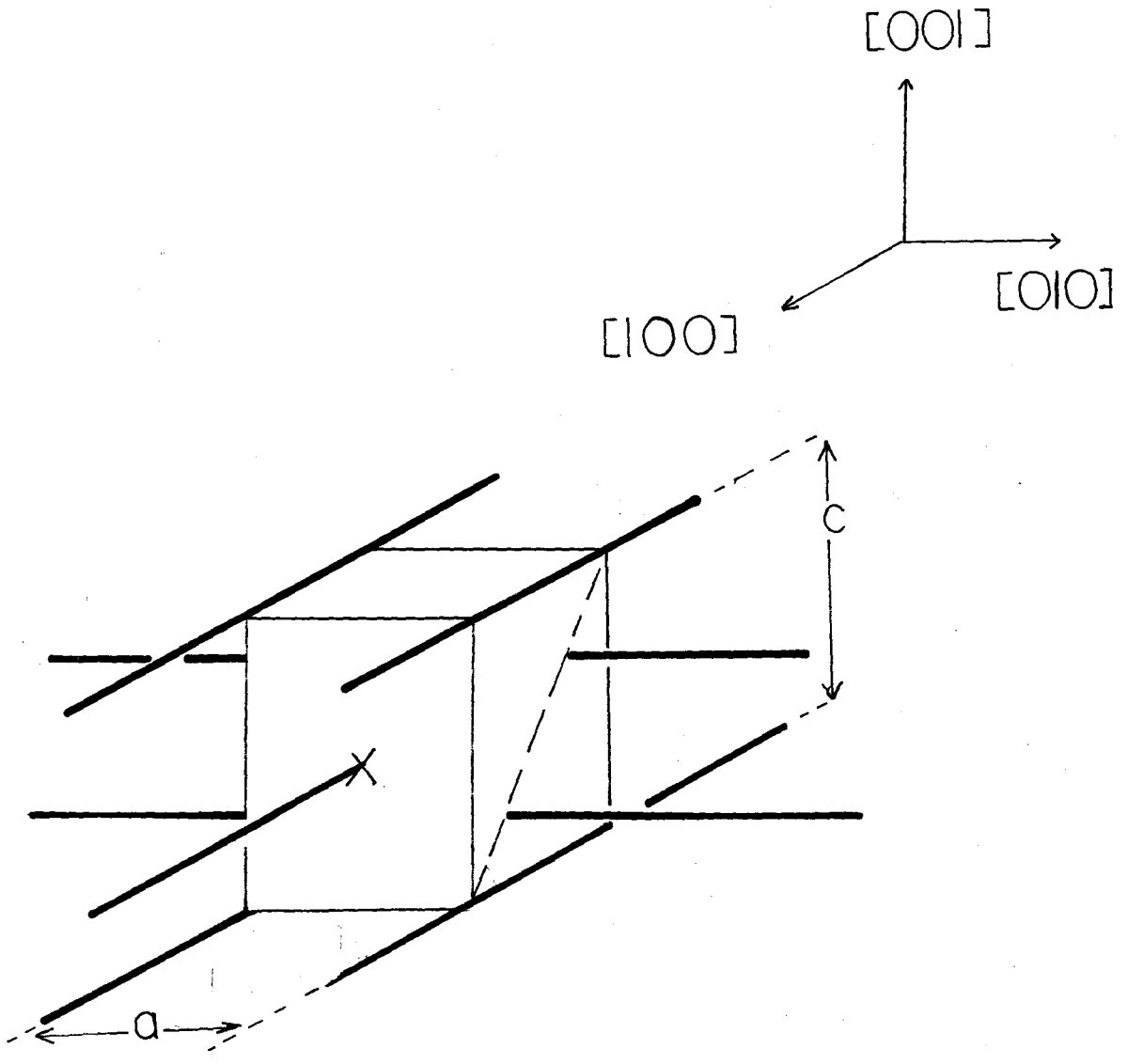

FIGURE 7.1: Heavy lines indicate Hg chain position and direction relative to the AsF_6^- unit cell, drawn as a solid block.

Table (7.1)

Crystal Parameters of $Hg_{3-\delta}AsF_6$

Parameter	Room Temperature (295 K)		10 K
a	7.538*Å	7.531 Å	7.443 Å
c	12.339*Å	12.395 Å	12.228 Å
Hg-Hg distance (along chain)	2.64*Å	2.670 Å	2.670 Å

*From Brown et al. (1974). All other entries are from Pouget et al. (1978).

space. By counting conduction electrons per unit cell and filling one dimensional electron states the Fermi wavevectors along the $\vec{a}$ and $\vec{b}$ directions are found to be $k_a = k_b = \pm 2.29\ \pi/a$, which are mapped to the first Brillouin zone, to $k_a = k_b = \pm 0.29\ \pi/a$. Interactions between crossed Hg chains introduce a splitting at the intersection of these Fermi surface planes to create a hole orbit (designated ε) and an

electron orbit (designated γ) in the (001) plane, shown in figure (7.2a). The perturbations introduced by Hg periodicity along a chain create splitting which are not necessary to this discussion: Razavi et al. observed the γ and ε orbits as well as orbits formed by the Hg-chain periodicity.

The Fermi surface has open orbits in the [001] direction with the magnetic field in the (001) plane, shown in figure (7.2b).

In all cases, induced torque measurements show one major peak which was observed with the magnetic field in the (001) plane. The field dependence of this peak ($B_o^{2.0\pm0.1}$) indicates it was produced by an open orbit since B_o^2 behaviour is expected in that case. The induced torque therefore shows that an open orbit lies in the [001] direction, in agreement with the Fermi surface model.

At angles 90° from the major peak, the induced torque is small and tends to saturate or increase linearly in magnetic field, characteristic of a closed orbit. The torque minimum (-50° in figure (6.1)) does not saturate as predicted for the ideal case for a closed orbit. However, the anomalous weak linearity in field has been observed in other metals (Douglas et al., 1970) and is attributed to the departure of magnetoresistance (ρ_{xx}) from ideal behaviour. Therefore the induced torque meaurements show only closed orbits with the magnetic field in the [001] direction.

The magnetic field dependence of the amplitude of subsidiary peaks does not indicate a simple open or closed orbit. Magnetic breakdown is a tunnelling of electrons across an energy gap from one part of the Fermi surface to another. The probability that this will occur can be written (Stark and Falicov, 1956)

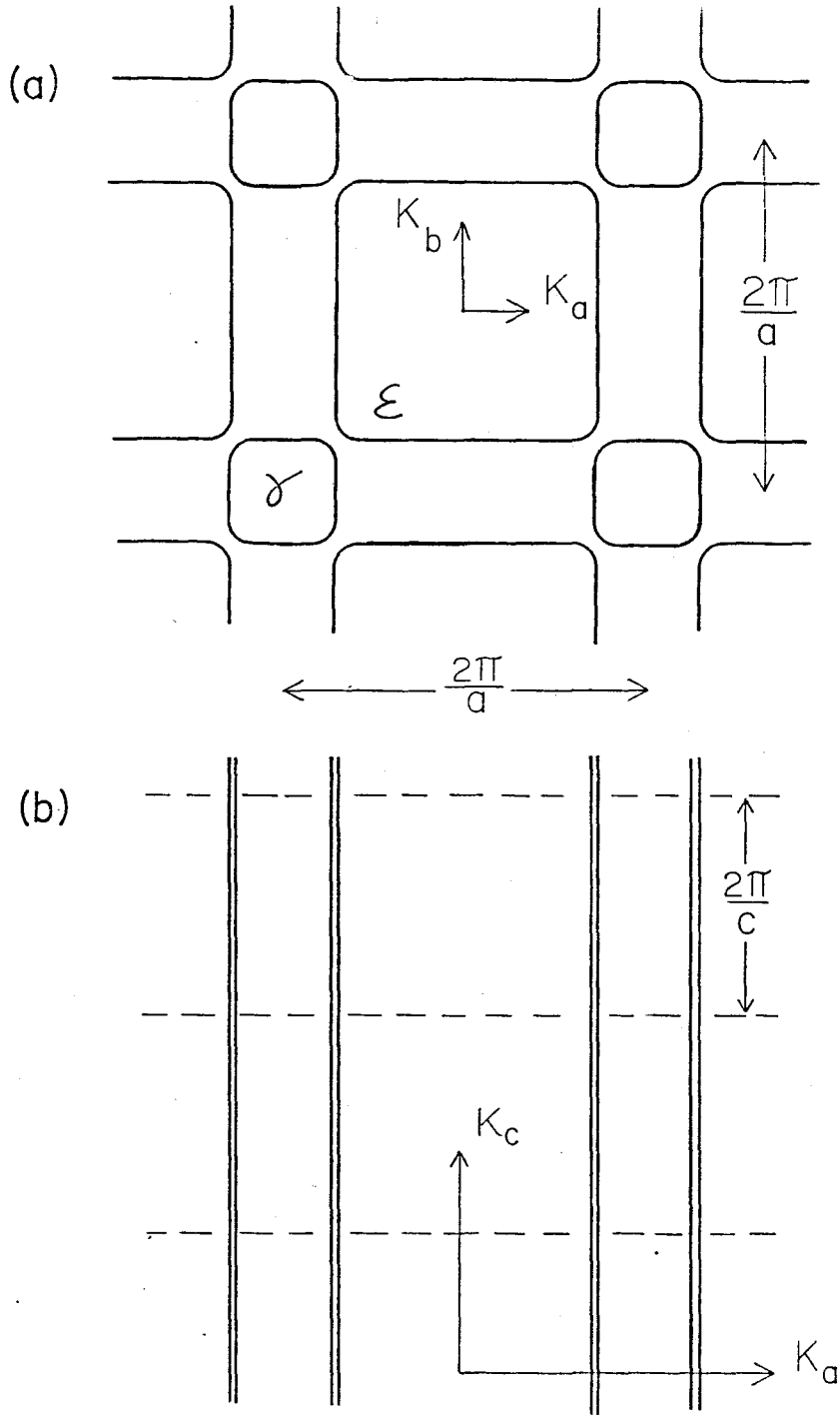

FIGURE 7.2: The Fermi surface of $Hg_{3-\delta}AsF_6$ formed from one dimensional bands (a) in the (001) plane and (b) in the (010) plane.

$$P = \exp\left(-\frac{\pi\varepsilon_g^2}{4\hbar\mu_o He|v_x v_y|}\right)$$

where H = magnetic field

ε_g = the size of the energy gap

v_x, v_y are components of electron velocity parallel and perpendicular to the gap.

Magnetic breakdown can produce an open orbit where none existed at low fields. Seivert and Falicov (1965) show that ρ_{xx} increases field B_o as $B_o^2 P$. In this case, the induced torque may be written

$$N = aB^o(1-P) + bB^2P$$

to account for closed orbits (the first term) and open orbits. This is a simplification because extended closed orbits will be created by magnetic breakdown, but the expression illustrates that N will rise in field faster than B_o^2. This describes the behaviour of the subsidiary peaks and therefore they are attributed to magnetic breakdown.

The stereographic projection of the positions of the subsidiary peaks (figure (6.6)) was constructed by placing the major peaks (due to a simple open orbit) in the (001) plane. Subsidiary peaks were mapped using their angles from the major peak. From the projection it is immediately clear from figure (7.2) that such peaks are due to open orbits perpendicular to planes of the form (mon).

Reciprocal lattice vectors and their angles from [100] are calculated using the crystal parameters of the AsF_6^- lattice, shown in Table (7.2). Matching the angles, planes perpendicular to open orbits

are (305), (407), (102), (307), (103), (207), (104), (105), (106), (107), (108), (1 0 13). More peaks exist, closer to the [001] direction, but several planes could be assigned to each so these are not included here. In each case, the experimental uncertainty is ±1°: the theoretical values match these angles within this uncertainty with the exception of (102) where the experimental figure is 49°±1° and the theoretical prediction is 50.5°. This value is within one and a half times the uncertainty which is acceptable here. The symmetry proposed does not predict peaks where none are found. In order to have such peaks, open orbits would be needed in directions of very high order reciprocal lattice vectors, and these are not likely to occur. Therefore, it is concluded that the open orbits produced by magnetic breakdown lie in symmetry directions of the tetragonal lattice. This confirms that the symmetry used by Razavi et al. is satisfactory.

For the flat sided Fermi surface model of Razavi et al., breakdown is equally possible at all points along k_c. To fulfill the symmetry demanded, breakdown must occur only at points along the Fermi surface spaced $\frac{2\pi}{c}$ apart.

An interaction between crossed chains, separated by a distance c/4, results in an energy gap (Batalla, 1981)

$$\varepsilon(\underset{\sim}{k}) = \varepsilon(k_x+k_y) + \delta\varepsilon \cos\left(\frac{k_z c}{4}\right)$$

This would introduce a periodicity along k_c of $\frac{2\pi}{c}$ because the energy gap is a minimum at $k_c = 0$ and a maximum at $k_c = \pm\frac{\pi}{c}$. Magnetic breakdown is expected to occur at $k_c = 0$. The interaction between crossed mercury chains also introduces an undulation in the Fermi

Table (7.2)

Angle Between [100] and Planes Containing Open Orbits

Experimental Value (in degrees ±1°)	Theoretical Prediction	Crystallographic Direction
45.0	45.3	(305)
47.5	46.7	(407)
49.0	50.5	(102)
54.0	54.7	(307)
59.5	61.1	(103)
65.0	64.8	(207)
66.0	67.5	(104)
71.7	71.9	(105)
74.5	74.6	(106)
77.0	76.7	(107)
79.5	78.4	(108)
82.5*	82.8	(1013)

*At very large angles many different ratios of c/a could be used with some direction assignment (nom).

surface cylinders. This indulation is too small to be observed by the dHvA effect.

There is no magnetic breakdown if $\vec{B}_o$ is parallel or perpendicular to the [001] direction, and the expression $N \sim \rho_{xx}/\rho_{xy}^2$ is of some use.

In the case that $\vec{B}_o$ is perpendicular to [001], the resistivity tensor element ρ_{xy} is very small. This is due to the fact that an electron can change it's $\vec{x}$ or $\vec{y}$ component of velocity very little, given the nearly straight-sided Fermi surface cylinders. At 8.5 T with position modulated with amplitude 0.25 degrees, frequency 6.0 Hz, the induced torque is $1.5 \pm 0.1 \cdot 10^{-6}$ Nm. The resistivity is calculated to be $1.4 \cdot 10^{-9}$ Ωm. Uncertainty in the dimensions of the sample limit the precision to an order of magnitude, 10^{-9} Ωm. This agrees with the low temperature value of ρ found by Cutforth et al., (1975).

Given $\rho = 10^{-9}$ Ωm, and using an effective mass 0.35 M_e (Razavi, 1979), τ is calculated to be $.5 \cdot 10^{-11}$ seconds. The value τ can be found in another way: N/B_o peaks at $\omega_c\tau=2$ if no open orbits are present (Martin Elliot, private communication). Using the data plotted in figure 6.3b, $\omega_c\tau=2$ at $B_o = 0.033 \pm .006$ T, therefore $\tau = 1.2 \pm 0.2 \cdot 10^{-10}$ seconds. These values of τ are different by a factor 2, but this may be accounted for by the fact that different samples were used.

The value τ determined at low fields is the more trustworthy: the high field value is found using $\sigma = \frac{ne^2\tau}{m_e}$, which may not describe this case completely.

If $\vec{B}_o$ is parallel to [001], given a nearly flat-sided Fermi surface σ_{xx} is the same as $\vec{B}_o$ perpendicular to [001]: also $\sigma_{yy} = \sigma_{xx}$. Contributions to σ_{zz} are made only by the component of electron velocity

in the [001] direction and σ_{zz} is therefore small. If it is assumed that no longitudinal-transverse mixing occurs [$\sigma_{iz} = \sigma_{zi} = 0$]. ρ_{zz} is very large and the approximation $\sigma_{zx}' \simeq \rho_{xx}/\rho_{xy}$ is probably invalid.

There are two cases:

$$\sigma_{xx}' \simeq \frac{\kappa B_o^2}{2\rho_{zz}} \quad ; \qquad \rho_{xx}\rho_{zz} > \rho_{xy}^2$$

or $$\sigma_{xx}' \simeq \kappa B_o^2 \frac{\rho_{zz}}{\rho_{xy}^2} \quad ; \; \rho_{xx}\rho_{zz} < \rho_{xy}^2$$

In the first case, the induced torque would show a B_o^2 dependence, which is not observed at this orientation. In the second case, closed orbit behaviour is expected with very large magnitude, also not observed. The simplest explanation is that the sample was not oriented with the [001] direction near $\vec{B}_o$. Then, σ_{zz} would be of the same order as σ_{xx} and the usual approximation $N \simeq \kappa B_o^2 \frac{\rho_{xx}}{\rho_{xy}^2}$ holds.

Using $\rho_{xx} = 10^{-9}$ Ωm and the ratio of the torque amplitudes between the major peak ($4.53 \pm .01 \cdot 10^{-5}$ N-m) and the minimum torque ($2.00 \pm .03 \cdot 10^{-7}$ Nm) at 8.5 T.

$$N_{peak} = 4.53 \pm .01 \cdot 10^{-5} \text{ N-m} = \frac{\kappa B_o^2 2}{\rho_{xx}}$$

$$N_{minimum} = 2.00 \pm .03 \cdot 10^{-7} \text{ N-m} = \kappa B_o^2 \frac{\rho_{xx}}{\rho_{xy}^2}$$

Therefore

$$1.26 \cdot 10^2 = 2 \frac{\rho_{xy}^2}{\rho_{xx}^2}$$

or $$\rho_{xy} = 7.94 \, \rho_{xx} \sim 8 \cdot 10^{-9} \text{ Ωm}$$

$$R_H = \frac{\rho_{xy}}{B_o} = 9 \cdot 10^{-10} \ \Omega m/T$$

This value is of the same order of magnitude as R_H for common metals.

The first observation of the de Haas van Alphen effect in this compound was obtained while making these induced torque measurements. The dHvA frequencies 604 T, 360 T reported in chapter 6 are within 20 T of the frequencies of the minimum Fermi surface cross section areas of the γ and α orbits reported by Razavi et al. (1979). However, Razavi reports no frequencies 724 T or 1032 T. It is most probable that the 724 T frequency is the second harmonic of the α frequency. The 1032 T could be the sum of the α and β frequencies (1039 T), within the limits of error here. It is possible that these orbits are due to extended closed orbits caused by magnetic breakdown but this is uncorroborated and these frequencies are regarded as harmonics or mixes.

CHAPTER 8

CONCLUSION

The possibility of systematic error introduced by position modulation in an induced torque experiment has been detailed in Chapter 4. It has been shown that a maximum systematic error of 5% in torque amplitude is expected to occur in the worst case of very high conductivity with no open orbits perpendicular to $\vec{B}_o$. A method of monitoring and limiting this error was presented.

It is shown in Chapter 3 that a phase reference line from the magnetometer position drive to the lockin amplifier reference circuit would eliminate the need for experimenter monitoring and adjustment, and also establish a more reliable zero-torque output voltage. Also, the Hall term of the resistivity tensor (ρ_{xy}) could be measured after a minor modification to the magnetometer. Several non-contact methods of measuring ρ_{xy} are known; however the induced torque magnetometer is a rapid survey device: further, in some circumstances the induced torque and ρ_{xy} could be used to find the magnetoresistance ρ_{xx}.

Induced torque measurements of $Hg_{3-\delta}AsF_6$ have shown a major peak due to an open orbit in the [001] direction, and only closed orbits in the (001) plane. This is in agreement with the Fermi surface model constructed by Razavi et al., (1979).

Subsidiary peaks were also observed. These peaks are due to magnetic breakdown between Fermi surface cylinders, and because discrete peaks are observed some modulation of the cylinders

undetected by Razavi and coworkers must occur. The angular position of subsidiary peaks confirms the tetragonal symmetry used by Razavi et al. in constructing the Fermi surface and shows that there is a small undulation that had not been detected.

The mean scattering time τ has been shown by low field measurements to be of order 10^{-10} seconds. The value R_H is of the same order of magnitude found in more common metals when $\vec{B}_o$ is not perpendicular to an open orbit.

BIBLIOGRAPHY

Balcombe, R.J., and Parker, R.A., Phil. Mag., 21, 533, (1970).

Barrett, C.S., Acta Cryst., 10, 58 (1957).

Batalla, E., Doctoral Thesis, unpublished, (1981).

Brown, I.D., Cutforth, B.D., Davies, C.G., Gillespie, R.J., Ireland, P.R, and Vekris, J., Can. J. Chem., 52, 791 (1974).

Chaing, C.K., Spal, R., Denenstein, A.M., Heeger, A.J., Miro, N.D., and McDiarmid, A.G., Solid State Commun., 22, 293 (1977).

Cutforth, B.D., Datars, W.R., van Schyndel, A., and Gillespie, R.J., Solid State Commun., 21, 377 (1976).

Cutforth, B.D., Datars, W.R., Gillespie, R.J., and van Schyndel, A., Adv. Chem., 150, 56 (1975).

Datars, W.R., Phys. Lett., A29, 700 (1969).

Delaney, J.A. and Pippard, A.B., Rep. Prog. Phys., 35, 671 (1972).

Dinser, R.J., Datars, W.R., Chartier, D., and Gillespie, R., Solid State Commun., 32, 1041 (1979).

Douglas, R.J. and Datars, W.R., Solid State Commun., 13, 839 (1973).

Elliott, M., and Datars, W.R., submitted to J. Phys. F., (1982).

Falicov, L.M., and Sievert, P.R., Phys. Rev., 138, A88, (1965).

Gillespie, R.J., and Ummat, P.K., Chem. Commun., 13, 839, (1973).

Gold, A.V., 1968, Solid State Physics, The Simon Fraser University Lectures, Vol. 1, Electrons in Metals, ed. by J.F. Cochran and R.R. Haering, Gordon and Breach, N.Y.

Goodman, J.M. Phys. Rev., 171, 641 (1968).

Hauser, W., Introduction to the Principles of Electromagnetism, Addison-Wesley, Don Mills, 1971.

Holroyd, F.W., Doublas, R.J., and Datars, W.R., Can. J. Phys., 51, 1786 (1973).

Koteles, E.S., Datars, W.R., Cutforth, B.D., and Gillespie, R.J., Solid State Commun., 20, 1129 (1976).

Kittel, C., Introduction to Solid State Physics, Wiley, N.Y. (1971).

Landau, L.D. and Lifshitz, E.M., Electrodynamics of Continuous Media, Pergamon Press, N.Y. (1960).

Lass, J.S. and Pippard, A.B., J. Phys. E: Sci. Instrum., 3, 137 (1970).

Lass, J.S., Phys. Rev. B, 13, 2247 (1976).

Peebles, D.L., Chiang, C.K., Cohen, M.J., Heeger, A.J., Miro, N.D. and MacDiarmid, A.G., Phys. Rev. B, 15, 9607 (1977).

Pouget, J.P., Shirane, G., Hastings, J.M., Heeger, A.J., Miro, N.D. and MacDiarmid, A.G., Phys. Rev. B, 18, 3645 (1978).

Razavi, F.S., Datars, W.R., Chartier, D., and Gillespie, R.J., Phys. Rev. Lett., 42, 1182 (1979).

Scholz, G.A., Datars, W.R., Chartier, D. and Gillespie, R.J., Phys. Rev. B, 16, 4209 (1977).

Stark, R.W. and Falicov, L.M., Prog. Low Temp. Phys., 5, 235 (1967).

Verge, C., Altounian, Z. and Datars, W.R., J. Phys. E., 10, 16 (1977).

Visscher, P.B. and Falicov, L.M., Phys. Rev. B, 2, 1518 (1970).

Ziman, J.M., Principles of the Theory of Solids, Cambridge University Press, London, (1964).